Incorporation of multi-phase halogen chemistry into Community Multiscale Air Quality (CMAQ) model

Kiyeon Kim[1], Chul Han Song[1*], Kyung Man Han[1], Greg Yarwood[2], Ross Beardsley[2], and Saewung Kim[3]

1. School of Earth Science and Environmental Engineering, Gwangju Institute of Science and Technology (GIST), Gwangju 61005, Republic of Korea
2. Ramboll, Novato, CA 94945, USA
3. Department of Earth System Science, University of California, Irvine, CA, USA

Shortened title: Multi-phase halogen chemistry

*Corresponding author: Chul Han Song (chsong@gist.ac.kr)

(Submitted to *Atmospheric Chemistry and Physics*)

Abstract

Halogen radicals (Cl, Br, and I) significantly influence atmospheric oxidation capacity, affecting both O_3 formation and destruction. However, understanding of halogen chemistry remains limited. To better investigate comprehensive atmospheric halogen chemistry, we incorporated halogen processes into the Community Multi-scale Air Quality (CMAQ) model: (i) emissions of Cl_2, HCl, Br_2, and HBr from anthropogenic sources, and Br_2, I_2, HOI, and halocarbons from natural sources; and (ii) 177 multi-phase halogen reactions. Model performance was evaluated against observed $ClNO_2$ levels, and by comparison with reported ranges of BrO and IO levels. The updated model showed significant improvements in simulating $ClNO_2$ mixing ratios, with the index of agreement (IOA) increasing from 0.41 to 0.66 and mean bias (MB) decreasing from -159.36 ppt to -25.07 ppt at supersites. Furthermore, simulated BrO and IO levels fell within the ranges reported in previous studies. We found that these improvements were driven by four key reactions: (i) ClO self-reaction, (ii) heterogeneous HOBr chemistry, (iii) NO_2 uptake, and (iv) revised N_2O_5 parameterization. Based on our modeling system, we found that the presence of halogen radicals led to changes in the net O_x production rate ($P(O_x)$), which increased from 3.08 ppb/h to 3.33 ppb/h on land and decreased from 0.21 ppb/h to 0.07 ppb/h over ocean. It was noted that levels of OH, HCHO, and NO_x also increased by ~0.007 ppt (5.5%), ~0.03 ppb (1.6%), and ~0.29 ppb (2.9%), respectively, while levels of HO_2 and VOCs decreased by ~0.45 ppt (5.3%) and ~0.71 ppb (5.9%). These results highlight the importance of accurately representing halogen processes in regional air quality models.

Keywords: Halogen chemistry; Anthropogenic halogen emission; Nitryl chloride ($ClNO_2$); Net O_x production ($P(O_x)$); Regional air quality;

1. Introduction

Atmospheric oxidants, such as OH, NO_3, and O_3, play a significant role in atmospheric chemistry. These oxidants react with volatile organic compounds (VOCs), leading to the formation of peroxyl radicals (RO_2), which, in turn, influences the O_3 formation. They also contribute to the formation of secondary organic and inorganic aerosols. Meanwhile, halogen radicals (such as Cl, Br, and I) also serve as oxidants in the atmosphere, affecting the oxidation capacity through various reactions (R1 – R4; see below) (Simpson et al., 2015; von Glasow and Crutzen, 2003; Fan and Li, 2022).

$$X \text{ (Cl, Br, and I)} + VOC \rightarrow RO_2 \tag{R1}$$
$$RO_2 + NO \rightarrow NO_2 + RO \tag{R2}$$
$$HO_2 + NO \rightarrow NO_2 + OH \tag{R3}$$
$$NO_2 \overset{hv}{\rightarrow} O^{3p} + O_2 \overset{M}{\rightarrow} O_3 \tag{R4}$$
$$X + O_3 \rightarrow XO + O_2 \tag{R5}$$
$$XO + HO_2 \rightarrow HOX + O_2 \tag{R6}$$
$$HOX \overset{hv}{\rightarrow} X + OH \tag{R7}$$

These radicals can also make substantial impacts on the O_3 loss via reactions (R5) – (R7) (Saiz-Lopez et al., 2012; Sarwar et al., 2015; Simpson et al., 2015). Given their roles in both the O_3 formation and destruction, a comprehensive understanding of atmospheric halogen chemistry is essential for accurately assessing the oxidative potentials of the atmosphere.

In this context, several studies attempted to incorporate chlorine chemistry into chemical-transport models (e.g., Yi et al., 2021; Sarwar et al., 2012; Qiu et al., 2019a and b). Specifically, Qiu et al. (2019a) reported that heterogeneous reactions involving reactive chlorine species can increase O_3 levels by approximately 20%. Moreover, Liu et al. (2018) found that the mixing ratios of O_3 increased by ~7.7 ppbv when anthropogenic chlorine emissions were included.

On the other hand, numerous studies have emphasized not only the significance of chlorine chemistry but also the influence of the synergistic effects of bromine and iodine chemistry with chlorine chemistry (Sarwar et al., 2019; Simpson et al., 2015; Caram et al., 2023; Badia et al., 2019; Saiz-Lopez et al., 2014; Li et al., 2022; Iglesias-Suarez et al., 2020). For instance, modeling studies considering both bromine and iodine chemistries showed that simulated O_3 levels actually decreased by 15.9 ppb (Parrella et al., 2012; Sarwar et al., 2015; Herrmann et al., 2022; Gantt et al., 2017; Read et al., 2008; Huang et al., 2021). These findings strongly suggest that incorporating chlorine processes, together with bromine and iodine processes, is crucial for correct and comprehensive understanding of atmospheric chemistry.

The Korean Peninsula, surrounded by the Yellow Sea, Korea Strait, and the East Sea, is characterized by high population density and highly industrial regions. Therefore, it can be influenced by both natural (oceanic) and anthropogenic halogen emissions. However, almost no modeling study has taken into account the natural and anthropogenic halogen processes over/around South Korea. Although almost no research has been carried out to examine the impacts of halogen chemistry on atmospheric composition over/around South Korea, several studies have considered atmospheric chlorine processes using 3D chemical-transport models (CTMs) (e.g., Jo et al., 2023; Kim et al., 2023). Given the synergistic effects of chlorine, bromine and iodine chemistries in the atmosphere, a comprehensive study that takes all these halogen processes into account is absolutely necessary.

For the comprehensive analysis of halogen processes and their influence on regional air quality, we established anthropogenic and natural halogen emissions and incorporated full sets of halogen reactions into the framework of the Community Multi-scale Air Quality (CMAQ) model. Specifically, we incorporated the following halogen processes into the CMAQ model: (i) atmospheric chlorine processes (anthropogenic HCl and Cl_2 emissions with 58 chlorine reactions); (ii) atmospheric bromine processes (anthropogenic and natural HBr and

97   Br$_2$ emissions together with 64 bromine reactions); and (iii) atmospheric iodine processes (HOI

98   and I$_2$ natural emissions, along with 55 iodine reactions).

99   Based on this modeling system, the primary objectives of this study are threefold: (i)

100   to develop and implement an updated halogen chemistry that accounts for the interactions

101   among multiple halogen species; (ii) to evaluate model performance using observational data

102   from the Korea US Air Quality (KORUS-AQ) campaign (1 May – 12 June, 2016), including

103   direct ClNO$_2$ measurements and inferred estimates of BrO and IO; and (iii) to examine the

104   atmospheric impacts of the updated halogen chemistry on a broader set of key atmospheric

105   constituents such as O$_3$, OH, HO$_2$, HCHO, VOC$_s$, and NO$_x$. In this context, this study is

106   designed to support a comprehensive understanding of atmospheric halogen processes and their

107   implications for regional air quality.

108

109   **2. Methodology**

110   In this study, we incorporated homogeneous, aqueous, and heterogeneous halogen

111   reactions into the CMAQ model, along with emissions of halogen species. To evaluate the

112   accuracy of these halogen processes, we compared the model results with observational data

113   from the KORUS-AQ campaign (Jeong et al., 2019; Crawford et al., 2021). This section

114   provides several details on the observation data, the WRF-CMAQ model configurations, and

115   the atmospheric halogen processes, including halogen reactions and emissions.

116   **2.1 Observation data**

117   Mixing ratios of nitryl chloride (ClNO$_2$) were measured every five minutes at Olympic

118   Park (37.52°N; 127.12°E) and Mt. Taewha (37.27°N; 127.41°E) stations during the period of

119   the KORUS-AQ campaign (refer to two blue stars in Fig. 1a), using Chemical Ionization Mass

120   Spectrometer (CIMS). The CIMS instrument has a detection limit of 1.5 ppt and an uncertainty

121   within 20%. Further details on the CIMS instrument are found in Slusher et al. (2004) and

122 Jeong et al. (2019). In our study, ClNO$_2$ observations were utilized to evaluate the performance

123 of the modified CMAQ model simulations. These results are discussed in Sect. 3.1.

2.2 WRF-CMAQ model description

125 The Weather Research and Forecasting (WRF) v3.8.1 model simulations were carried

126 out to generate meteorological fields (Skamarock et al., 2008). The details of physical

127 parameters used in the WRF simulations are summarized in Table S1. National Center for

128 Environmental Prediction Final Analysis (NCEP-FNL) data were used for initial and boundary

129 conditions. The WRF model included a 5-day spin-up period to minimize uncertainties from

130 the initial and boundary conditions.

131 This study also included the CMAQ v5.2.1 model simulations (Byun and Schere, 2006)

132 over a domain covering northeast Asia with 273 × 204 horizontal grid cells. The grid

133 resolution is 15 × 15 km^2 with 15 vertical layers from surface to 50 hPa. The Statewide Air

134 Pollution Research Center-07 (SAPRC-07TC) mechanism (Carter, 2010; Hutzell et al., 2012)

135 with AERO6 module was used in the CMAQ model simulations. One limitation of the SAPRC-

136 07TC mechanism is that it has only basic chlorine chemistry. In order to implement more

137 sophisticated halogen model simulations, we incorporated additional and updated halogen

138 reactions into the SAPRC-07TC mechanism. The detailed reactions are explained in Sects.

139 2.4.1 and 2.4.2.

140 In order to run the CMAQ model, biomass burning and biogenic emissions were

141 obtained from the Fire Inventory from NCAR (FINN) v1.5 (Wiedinmyer et al., 2011) and the

142 Model of Emissions of Gases and Aerosol from Nature (MEGAN) v2.1 (Guenther et al., 2012),

143 respectively. Anthropogenic emissions were acquired from the KORUS v5.0 emission

144 inventory (Woo et al., 2020), specifically developed for the KORUS-AQ campaign. The

145 KORUS v5.0 inventory covers emissions of primary pollutants such as NO$_x$, CO, HCHO,

146 VOCs, and particulate chlorine (pCl$^-$), but it omits the emissions for anthropogenic chlorine

147 species (HCl and Cl_2), bromine species (HBr and Br_2), and ocean-generated halogen species

148 (HOI, I_2, and halocarbons). We have thus developed new halogen emissions for this study. The

149 methodology for developing the halogen emissions will be discussed in Sections 2.3.1 and

150 2.3.2.

2.3 Halogen emissions

152   In this section, we discuss the development of anthropogenic and natural halogen

153 emissions within our model framework.

2.3.1 Anthropogenic emissions

155   First, we assumed that emissions of anthropogenic HCl and Cl_2 mainly originated from

156 coal combustion. Coal combustion occurs predominantly in four main sectors: industry,

157 residential areas, power plants, and other sectors such as agriculture and furniture

158 manufacturing. In addition, HCl emissions also take place from municipal solid waste

159 incineration.

160   To calculate chlorine emissions from industry and residential areas, we utilized coal

161 consumption data from the 2016 Regional Energy Report of South Korea

162 (https://www.keei.re.kr). Thereafter, the emissions of HCl and Cl_2 from these sectors were

163 calculated using the following equation (1):

164    $$E_{i,j} = M_{i,j} \times EF_{i,j} \times \rho \times \frac{1}{MM} \times \frac{1}{10^3}$$   (Eq. 1)

165 where $E_{i,j}$ represents the emission for species i in categories j (Mg); M denotes the coal

166 consumption (Gg); and EF is the emission factor (µg/g) calculated using the method from a

167 previous study (Jiang et al., 2005 (in Chinese)). ρ indicates the percentage of HCl and Cl_2 in

168 the chlorine content of coal. In our study, percentages of 86.3% and 3.63% for ρ_{HCl} and ρ_{Cl2}

169 were used, respectively, based on research conducted by Deng et al. (2014) and Liu et al. (2018).

170 MM represents the ratios of the molar mass of the chlorine atom to the molecular weight (i.e.,

171 35.5/36.5 for HCl and 1 for Cl_2).

172   For the remaining three sectors, namely power plants, solid waste incineration, and

173   others, the HCl emissions were obtained directly from the Korean tele-monitoring system

174   (TMS) named the CleanSYS (https://cleansys.or.kr). Meanwhile, the emissions of Cl_2 from

175   these sectors can also be calculated using equation (1), based on the HCl emissions previously

176   calculated.

177   Bromine emissions (HBr and Br_2) were additionally estimated from the previously

178   calculated chlorine emissions. According to a recent study, bromine is also emitted from the

179   coal combustion with a ratio (0.25) of bromine to chlorine concentrations (Peng and Wu, 2014).

180   These bromine emissions were split into 70% and 30% for HBr and Br_2, respectively. The

181   detailed methodology used in our study is summarized in Li et al. (2021).

182   Consequently, we developed an emission inventory that includes anthropogenic

183   chlorine and bromine emissions. Figure 1 illustrates the spatial distributions of these emissions

184   across South Korea. The total emission rates for anthropogenic HCl, Cl_2, HBr, and Br_2 in South

185   Korea are 5,989.6, 450.8, 460.8, and 240.8 $Mg \cdot yr^{-1}$ respectively. These values are higher than

186   those reported in previous studies conducted for the same region and time period. For instance,

187   Jo et al. (2023) estimated that total annual anthropogenic HCl emissions were less than 1.0 Gg,

188   whereas Kim et al. (2023) reported a value of 1.35 Gg. These discrepancies may result from

189   the inclusion of additional HCl emissions from the residential and industrial sectors in our study.

190   Moreover, our research also accounts for emissions of Cl_2, HBr, and Br_2. It is noteworthy that

191   Cl_2, HBr, and Br_2 have relatively shorter e-folding lifetimes (a few minutes for Cl_2 and Br_2,

192   and a few hours for HBr) than HCl (about 1.5 days), which may increase the oxidant capacity

193   in the atmosphere.

194
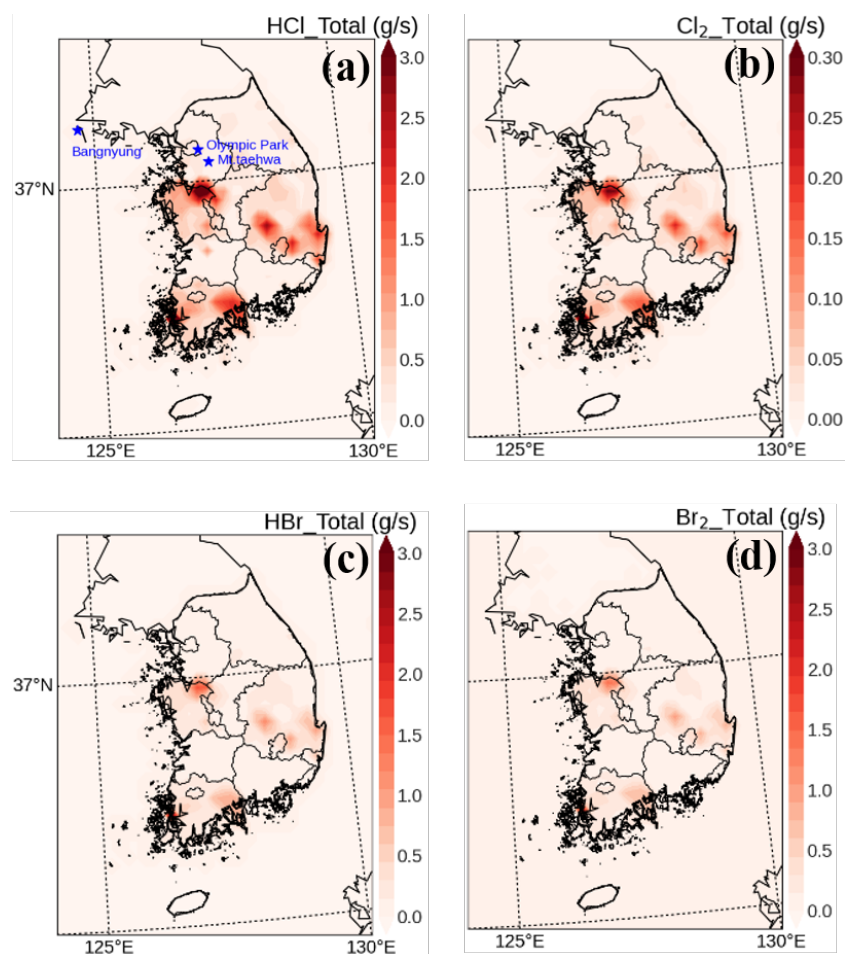
195 **Figure 1.** Spatial distributions of anthropogenic emission rates of (a) HCl, (b) Cl$_2$, (c) HBr, and
196 (d) Br$_2$ during the period of the KORUS-AQ campaign over South Korea. Three blue stars
197 denote the locations of three supersites (Bangnyung, Olympic Park, and Mt. Taehwa) during
198 the KORUS-AQ campaign.

199
200 **2.3.2 Natural emissions**

201   Biogenic halocarbons, such as CHBr$_3$, CH$_2$Br$_2$, CHBrCl$_2$, CH$_2$BrCl, CHBr$_2$Cl, CH$_2$I$_2$,

202 CH$_3$I, CH$_2$ICl, and CH$_2$IBr, are emitted from micro-algae activities in the ocean. To calculate

203 these emissions of bromine and iodine-containing halocarbon species, we used the chlorophyll-

204 a (chl-a) concentrations as a proxy for the photosynthetic activity of phytoplankton (Liss et al.,

205 2014).

206   Chlorophyll-a concentrations in the ocean have been monitored by various satellite

207 sensors such as Moderate Resolution Imaging Spectroradiometer (MODIS) and Geostationary

208 Ocean Color Imager (GOCI) (Kim et al., 2016; O'reilly and Werdell, 2019; Sarwar et al., 2015).

209   Among these sensors, Park et al. (2015) reported that the chlorophyll-a concentrations

210   measured by the GOCI sensor showed the best agreement with surface observations compared

211   to those from the MODIS sensor in the East Asian ocean. Based on this study, we applied the

212   chlorophyll-a data from the GOCI sensor into our study (refer to Fig. S1).

213   Gridded halocarbon emissions were estimated using the following equation (2)

214   (Sarwar et al., 2015):

215         $E_{Halocarbon} = 1.2 \times 10^{-11} \times (O_F + S_F) \times A_{GC} \times f_{HC} \times f_{DP} \times [chl\text{-}a]$ (Eq.2)

216   where O_F and S_F represent the ocean and coastal fractions of the grid cell, respectively. A_{GC}

217   denotes the area of the grid cell (m^2). f_{HC} is the emission factor for the species; and f_{DP}

218   represents the diurnal profile. [$chl\text{-}a$] denotes the chlorophyll-a concentration. The distributions

219   of natural bromine and iodine emissions are shown in Fig. S2.

220   Natural Br_2 emissions were estimated by debromination of sea-salt aerosols (SSAs),

221   following the method proposed by Sarwar et al. (2015) and Yang et al. (2005). In this approach,

222   Br^- contained within the SSAs was released into the atmosphere as Br_2 (i.e., dehalogenation of

223   SSAs). This process was parameterized based on sea-salt aerosol mass, Br/NaCl mass ratio,

224   sea surface temperature, and 10-m wind speed. In addition, inorganic iodine (such as HOI and

225   I_2) emissions were calculated at the air-sea water interfaces, utilizing information on dry

226   deposition of O_3 over the ocean. This approach is based on the fact that the formations of HOI

227   and I_2 are initiated by reaction between iodide (I^-(aq)) and O_3 at the ocean surfaces. More

228   detailed information on natural inorganic emissions can be found in Sarwar et al. (2015).

229   **2.4 Halogen chemical reactions**

230   As mentioned previously, the conventional CMAQ v5.2.1 model accounts for only a

231   limited set of chlorine-related processes: (i) reactions between VOCs and Cl radicals (Sander

232   et al., 2010), (ii) a simplified reactive chlorine cycling mechanism (Sander et al., 2010), and

233   (iii) the uptake of N_2O_5 on the chloride-containing particles (Bertram and Thornton, 2009).

234   Therefore, we attempted to incorporate the multi-phase halogen reactions into the CMAQ

235   v5.2.1 model to investigate the influences of atmospheric halogen chemistry. Detailed

236   descriptions of these reactions are provided in the subsequent sections.

237   **2.4.1 Chlorine reactions**

238   The chlorine-related reactions were incorporated into the framework of SAPRC07-TC

239   mechanism. The chlorine reactions consist of: (i) adjusted reaction rate coefficients for 14

240   reactions (refer to R9 to R22 in Table 1); (ii) updated 29 gaseous chlorine reactions (refer to

241   R23 to R51 in Table 1); (iii) added two aqueous-phase reactions (refer to R1 to R2 in Table 2);

242   and (iv) incorporated four heterogeneous reactions involving three reactive halogen species,

243   HOCl, ClNO$_2$, and ClONO$_2$, with NO$_2$ partitioning onto chloride-containing particles (refer to

244   R2 to R6 in Table 3).

245   The parameterization of γ_{N2O5} currently embedded in the CMAQ v5.2.1 model

246   (shown in R8) has not been greatly satisfactory for reproducing the atmospheric levels of

247   ClNO$_2$.

248    $$N_2O_5 + (1-\varphi)H_2O + \varphi Cl^{-1} \xrightarrow{\gamma_{N2O5}} (2-\varphi)HNO_3 + \varphi ClNO_2 \qquad (R8)$$
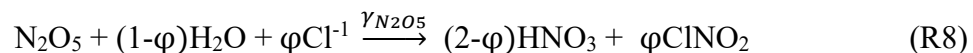
249   where φ represents the yield of ClNO$_2$ as a function of the concentration of particulate

250   chloride [Cl$^-$] and aerosol water content [H$_2$O]. The calculation of φ was proposed by Bertram

251   and Thornton (2009):

252    $$\varphi = \frac{1}{1+\frac{[H2O]}{483[Cl-]}} \qquad (Eq.\ 3)$$

253   Although the use of R8 and Eq. 3 have been an advance in considering the production

254   of ClNO$_2$ from chlorine-containing particles (Bertram and Thornton, 2009), several studies

255   have reported that the parameterizations of γ_{N2O5} with R8 and Eq. 3 tend to produce excessive

256   amounts of nitrate and ClNO$_2$ (Riedel et al., 2012a; Li et al., 2016; Yu et al., 2020). This

257   overestimation may result from uncertainties in calculating aerosol water content ([H$_2$O])

258 estimated from the aerosol thermodynamic module (Chang et al., 2016). To deal with this issue,

259 several studies have explored different parameterizations of γ_{N2O5}. However, the γ_{N2O5} still

260 appears to be over-estimated in many cases (e.g., Chang et al., 2016; Liu et al., 2019; Mcduffie

261 et al., 2018; Riedel et al., 2012a; Wang et al., 2017). In this context, we alternatively selected

262 a different parameterization for γ_{N2O5} (see equations (4) to (7)). These parameterizations

263 were suggested by Riemer et al. (2003) and Evans and Jacob (2005):

$$\gamma_{N2O5} = f \times \gamma_1 + (1-f) \times \gamma_2 \qquad \text{(Eq. 4)}$$

$$f = \frac{m_{sulfate}}{m_{sulfate} + m_{nitrate}} \qquad \text{(Eq. 5)}$$

$$\gamma_1 = \alpha \times 10^{\beta} \qquad \text{(Eq. 6)}$$

$$\gamma_2 = 0.1 \times \gamma_1 \qquad \text{(Eq. 7)}$$

268 where α is set to be $2.79 \times 10^{-4} + 1.3 \times 10^{-4} \times RH - 3.43 \times 10^{-4} \times RH^2 + 7.52 \times 10^{-8} \times RH^3$.

269 β is set at 0.48, when T < 282 K, or at $4 \times 10^{-2} \times (294 - T)$, when T $\geq$ 282 K. m_i represents

270 the aerosol mass concentration of species i. Complete lists of chlorine reactions embedded into

271 the SAPRC07TC mechanism are shown in Tables 1, 2, and 3.

272 **Table 1.** List of homogeneous chlorine reactions used in this study.

No	Reaction	Reaction rate	Reference
R1	$Cl_2 \xrightarrow{h\nu} 2Cl$	#1.0/<Cl$_2$>	1
R2	$ClNO \xrightarrow{h\nu} Cl + NO$	#1.0/<ClNO>	1
R3	$Cl + NO_2 + M = ClONO$	1.3e-30^-2.0&1.0e-10^-1.0&-1.0&0.6&1.0	1
R4	$Cl + NO_2 + M = ClNO_2$	1.8e-31^-2.0&1.0e-10^-1.0&-1.0&0.6&1.0	1
R5	$ClONO \xrightarrow{h\nu} Cl + NO_2$	#1.0/<ClONO>	1
R6	$Cl + NO_3 = ClO + NO_2$	2.4×10^{-11}	1
R7	$ClO + NO_2 = ClONO_2$	1.80e-31^-3.4&1.5e-11^-1.90&0.6&1.0	1
R8	$HOCl \xrightarrow{h\nu} Cl + OH$	#1.0/<HOCl>	1
R9	$ClONO_2 = Cl + NO_3$	#1.0/<ClONO$_{2\_1}$>	2
R10	$ClONO_2 = ClO + NO_2$	#1.0/<ClONO$_{2\_2}$>	2
R11	$Cl + NO + M = 2ClNO$	$7.70 \times 10^{-32}(\frac{T}{300})^{-1.8}$	2
R12	$ClNO_2 \xrightarrow{h\nu} Cl + NO_2$	#1.0/<ClNO$_2$>	2
R13	$Cl + HO_2 = HCl$	$1.4 \times 10^{-11}e^{270/T}$	2
R14	$Cl + HO_2 = ClO + OH$	$3.6 \times 10^{-11}e^{-375/T}$	2
R15	$Cl + O_3 = ClO$	$2.3 \times 10^{-11}e^{200/T}$	2
R16	$ClO + NO = Cl + NO_2$	$6.4 \times 10^{-12}e^{290/T}$	2
R17	$ClONO_2 = ClO + NO_2$	2.0×10^{-21}	2
R18	$Cl + ClONO_2 = Cl_2 + NO_3$	$6.5 \times 10^{-12}e^{135/T}$	2
R19	$ClO + HO_2 = HOCl$	$2.6 \times 10^{-12}e^{290/T}$	2
R20	$ClO + ClO = Cl_2 + O_2$	$1.0 \times 10^{-11}e^{-1590/T}$	2
R21	$OH + HCl = Cl$	$1.8 \times 10^{-12}e^{-250/T}$	2
R22	$Cl + H_2 = HCl + HO_2$	$3.1 \times 10^{-11}e^{-2270/T}$	2
R23	$ClO + O = Cl + O_2$	$2.8 \times 10^{-11}e^{85/T}$	2
R24	$ClO + OH = Cl + HO_2$	$7.4 \times 10^{-12}e^{270/T}$	2
R25	$ClO + OH = HCl + O_2$	$6.0 \times 10^{-13}e^{230/T}$	2
R26	$HOCl + OH = ClO + H_2O$	$3.0 \times 10^{-12}e^{-500/T}$	2
R27	$HOCl + O = ClO + OH$	1.7×10^{-13}	2
R28	$ClNO_2 + OH = HOCl + NO_2$	$2.4 \times 10^{-12}e^{-1250/T}$	2
R29	$ClONO_2 + O = ClO + NO_3$	$3.6 \times 10^{-12}e^{-840/T}$	2
R30	$ClONO_2 + OH = HOCl + NO_3$	$1.2 \times 10^{-12}e^{-330/T}$	2
R31	$HCl + O = Cl + OH$	$1.0 \times 10^{-11}e^{-3300/T}$	2
R32	$Cl + ClNO = NO + Cl_2$	$5.8 \times 10^{-11}e^{100/T}$	2
R33	$Cl + HOCl = OH + Cl_2$	$3.4 \times 10^{-12}e^{-130/T}$	2
R34	$ClO \xrightarrow{h\nu} Cl + O$	#1.0/<ClO>	2
R35	$Cl + H_2O_2 = HCl + HO_2$	$1.1 \times 10^{-11}e^{-980/T}$	2
R36	$OH + Cl_2 = HOCl + Cl$	$2.6 \times 10^{-12}e^{-1100/T}$	2
R37	$Cl + HNO_3 = HCl + NO_2$	2.0×10^{-16}	2
R38	$Cl_2O_2 \xrightarrow{h\nu} Cl + ClO_2$	#1.0/<Cl$_2$O$_2$>	2
R39	$ClO_2 \xrightarrow{h\nu} ClO + O_2$	#1.0/<ClO$_2$>	2
R40	$Cl + ClO_2 = 2ClO$	1.2×10^{-11}	2
R41	$Cl + ClO_2 = Cl_2 + O_2$	2.3×10^{-10}	2
R42	$OH + Cl_2O_2 = HOCl + ClO_2$	$6.0 \times 10^{-13}e^{670/T}$	2
R43	$OH + ClO_2 = HOCl + O_2$	$1.4 \times 10^{-12}e^{600/T}$	2
R44	$Cl_2 + O_2 + M = Cl_2O_2$	2.2e-33^3.1&1.8e-10^0&-1.0&0.6&1.0	2
R45	$ClO + ClO + M = ClO_2$	1.9e-32^3.6&3.7e-12^1.6&-1.0&0.6&1.0	2
R46	$ClO_2 + O = ClO$	$2.4 \times 10^{-12}e^{-960/T}$	2
R47	$NO + ClO_2 = ClO + NO_2$	$6.0 \times 10^{-13}e^{-670/T}$	2
R48	$HCl + NO_3 = HNO_3 + Cl$	5.0×10^{-17}	2
R49	$Cl + Cl_2O_2 = Cl_2 + ClO$	$6.2 \times 10^{-11}e^{130/T}$	2
R50	$ClO + O_3 = ClO_2$	$2.0 \times 10^{-12}e^{-3600/T}$	2
R51	$ClO + NO_3 = ClO_2 + NO_2$	4.7×10^{-13}	2

273   1. Sander et al. (2010); 2. Burkholder et al. (2020)

274 **Table 2.** List of aqueous-phase chlorine and bromine reactions used in this study.

No	Species	Reaction	Reaction rate (unit: M/s)	Reference
R1	HOCl	$HOCl + HSO_3^- \xrightarrow{k} SO_4^{2-} + Cl^- + 2H^+$	2.8×10^5	1
R2	HOCl	$HOCl + SO_3^{2-} \xrightarrow{k} SO_4^{2-} + HCl$	7.6×10^8	1
R3	HOBr	$HOBr + HSO_3^- \xrightarrow{k} SO_4^{2-} + HBr$	5.0×10^9	1
R4	HOBr	$HOBr + SO_3^{2-} \xrightarrow{k} SO_4^{2-} + HBr$	2.6×10^7	1

275 1. Liu and Abbatt. (2020)
276
277

278 **Table 3**. List of heterogeneous halogen reactions and the uptake coefficients of gases used in
279 this study.

No	Gas	Reaction	Uptake Coefficient (γ_{gas})	Reference
R1	N_2O_5	$N_2O_5 + (1-\varphi)H_2O + \varphi Cl^- \rightarrow (2-\varphi) HNO_3 + \varphi ClNO_2$	Function of aerosol mass concentrations, relative humidity, and temperature	1, 2
R2	HOCl~~HOCl~~	$HOCl + Cl^- = Cl_2$	1.09×10^{-3}	3
R3	$ClONO_2$	$ClONO_2 + Cl^- = Cl_2 + NO_3^-$	0.002	4
R4	$ClNO_2$	$ClNO_2 + Cl^- + H^+ = Cl_2 + HONO$	2.65×10^{-6} (pH < 2.0)	5
R5	$ClNO_2$	$ClNO_2 = Cl^- + NO_3^- + 2H^+$	6×10^{-6} (pH > 2.0)	6
R6	NO_2	$2NO_2 + Cl^- = ClNO~~ClNO~~ + NO_3^-$	10^{-4}	7
R7	HOBr~~HOBr~~	$HOBr + Br^- = Br_2$	0.08	8
R8	HOBr	$HOBr + Cl^- = BrCl$	0.02	8
R9	$BrONO_2$	$BrONO_2 + H_2O = HOBr~~HOBr~~ + HNO_3$	0.03	9
R10	HBr	$HBr = Br^-$	$1.3 \times 10^{-8} e^{\frac{4290}{T}}$	10
R11	$IONO_2$	$IONO_2 + Cl^- = ICl + HNO_3$	0.005	11
R12	$IONO_2$	$IONO_2 + Br^- = IBr + HNO_3$	0.005	11
R13	INO_2	$INO_2 + Cl^- = ICl + HONO$	0.01	11
R14	INO_2	$INO_2 + Br^- = IBr + HONO$	0.01	11
R15	HOI~~HOI~~	HOI~~HOI~~ $+ Cl^- = ICl$	0.005	12
R16	HOI~~HOI~~	HOI~~HOI~~ $+ Br^- = IBr$	0.005	12
R17	I_2O_2	$I_2O_2 =$	0.02	12
R18	I_2O_3	$I_2O_3 =$	0.02	12
R19	I_2O_4	$I_2O_4 =$	0.02	12

280 1. Riemer et al. (2003); 2. Evans and Jacob (2005); 3.Pratte and Rossi (2006); 4.Chen et al. (2022); 5.Riedel et al.
281 (2012); 6.Roberts et al. (2009); 7.Abbatt and Waschewsky (1998); 8.Fernandez et al. (2014); 9.Deiber et al. (2004);
282 10.Ammann et al. (2013); 11.Saiz Lopez et al. (2014); 12.Sherwen et al. (2016)

2.4.2 Bromine reactions

We also incorporated bromine reactions into the SAPRC07-TC mechanism. The reactions incorporated include: (i) updated absorption cross-sections for BrCl, BrCHO, $CHBr_2Cl$, $CHBr_3$, and $CHBrCl_2$ (refer to R29 to R33 in Table 4); (ii) updated reaction rates for formaldehyde (HCHO) and acetaldehyde (CH_3CHO) reacting with bromine radicals (refer to R34 and R35 in Table 4); (iii) Br-initiated VOC reactions (refer to R36 to R56 in Table 4); (iv) two inter-halogen species reactions (refer to R57 and R58 in Table 4); (v) two aqueous-phase reactions (refer to R3 to R4 in Table 2); and (vi) four heterogeneous reactions for bromine species (refer to R7 to R10 in Table 3). A complete list of the bromine reactions can be found in Tables 2, 3, and 4.

293   **Table 4**. List of homogeneous bromine reactions used in this study.

No	Reaction	Reaction rate	Reference
R1	$BrO \xrightarrow{hv} Br + O^3P$	#1.0/<BrO>	1
R2	$HOBr \xrightarrow{hv} Br + OH$	#1.0/<HOBr>	1
R3	$BrNO_3 \xrightarrow{hv} Br + NO_3$	#1.0/<BrNO$_3$_1>	1
R4	$BrNO_3 \xrightarrow{hv} BrO + NO_2$	#1.0/<BrNO$_3$_2>	1
R5	$BrNO_2 \xrightarrow{hv} Br + NO_2$	#1.0/<BrNO$_2$>	1
R6	$Br_2 \xrightarrow{hv} 2Br$	#1.0/<Br$_2$>	1
R7	$Br + O_3 = BrO$	$1.6 \times 10^{-11}e^{-780/T}$	1
R8	$BrO + HO_2 = HOBr$	$4.5 \times 10^{-12}e^{460/T}$	1
R9	$Br + HO_2 = HBr$	$4.8 \times 10^{-12}e^{-310/T}$	1
R10	$HBr + OH = Br$	$6.7 \times 10^{-12}e^{155/T}$	1
R11	$BrO + BrO = 2Br$	$1.4 \times 10^{-12}e^{210/T}$	1
R12	$BrO + BrO = Br_2$	$2.9 \times 10^{-14}e^{840/T}$	1
R13	$BrO + NO = Br + NO_2$	$8.8 \times 10^{-12}e^{260/T}$	1
R14	$Br + BrNO_3 = Br_2 + NO_3$	4.9×10^{-11}	1
R15	$Br_2 + OH = HOBr + Br$	$2.1 \times 10^{-11}e^{240/T}$	1
R16	$BrO + OH = Br + HO_2$	$1.7 \times 10^{-11}e^{250/T}$	1
R17	$Br + NO_3 = BrO + NO_2$	1.6×10^{-11}	1
R18	$BrO + ClO = Br + Cl$	$4.7 \times 10^{-12}e^{320/T}$	1
R19	$BrO + MEO2 = 0.8HOBR + 0.2BR + 0.3HCOOH + 0.2HCHO + 0.13OH + 0.13HO_2$	$2.65 \times 10^{-14}e^{1600/T}$	1
R20	$CH3Br + OH = Br$	$1.42 \times 10^{-12}e^{-1150/T}$	1
R21	$MB3^a + OH = 3Br$	$9.0 \times 10^{-13}e^{-360/T}$	1
R22	$MB2^b + OH = 2Br + HO_2$	$2.0 \times 10^{-12}e^{-840/T}$	1
R23	$MB2C^c + OH = 2Br + Cl$	$9.0 \times 10^{-13}e^{-420/T}$	1
R24	$MBC2^d + OH = Br + 2Cl$	$9.4 \times 10^{-13}e^{-510/T}$	1
R25	$MBC2^e + OH = Br + Cl + HO_2$	$2.1 \times 10^{-12}e^{-880/T}$	1
R26	$DMS + BrO = 0.75SO_2 + 0.25MSA + MEO2 + Br$	$1.5 \times 10^{-14}e^{1000/T}$	1
R27	$BrO + NO_2 = BrNO_3$	5.2e-31^3.2&6.9e-12^-2.9&0.6&1.0	1
R28	$Br + NO_2 = BrNO_2$	4.2e-31^2.4&2.7e-11^0.0&0.6&1.0	1
R29	$BrCl \xrightarrow{hv} Br + Cl$	#1.0/<BrCl>	2
R30	$FMBR^f \xrightarrow{hv} Br + CO + HO2$	#1.0/<FMBR>	2
R31	$MB3^a \xrightarrow{hv} 3.0Br + HO_2$	#1.0/<MB3>	2
R32	$MB2C^c \xrightarrow{hv} 2.0Br + Cl + HO_2$	#1.0/<MB2C>	2
R33	$MBC2^d \xrightarrow{hv} Br + 2.0Cl + HO_2$	#1.0/<MBC2>	2
R34	$HCHO + Br = HBr + HO_2$	$7.7 \times 10^{-12}e^{-580/T}$	2
R35	$CCHO + Br = HBr + MECO_3$	$1.8 \times 10^{-11}e^{-460/T}$	2
R36	$ETHE + Br = FMBR^f + HCHO + HO2 + RO2C$	1.3×10^{-13}	2
R37	$OLE1 + Br = FMBR^f + CCHO + HO2 + RO2C$	3.6×10^{-12}	2
R38	$OLE2 + Br = FMBR^f + 0.75RCHO + 0.15ACET + 0.1MEK + HO2 + RO2C$	1.0×10^{-11}	2
R39	$ISOPRENE + Br = FMBR^f + PRD2 + HO2 + RO2C$	7.5×10^{-11}	2
R40	$FMBR^f + OH = Br + CO$	5.0×10^{-12}	2
R41	$RCHO + Br = HBr + RCO3$	$1.8 \times 10^{-11}e^{-460/T}$	2
R42	$GLY + Br = HBr + 2CO + HO2$	$7.7 \times 10^{-12}e^{-580/T}$	2
R43	$MGLY + Br = HBr + CO + MECO3$	$1.8 \times 10^{-11}e^{-460/T}$	2
R44	$BALD + Br = HBr + BZCO3$	$1.8 \times 10^{-11}e^{-460/T}$	2
R45	$ACROLEIN + Br = 0.75 FMBR^f + 0.25HBr + 0.25MACO3 + 0.75MGLY + 0.75HO2$	1.0×10^{-11}	2
R46	Benzene + Br = Product	1.0×10^{-11}	3
R47	Toluene + Br = Product	1.0×10^{-14}	4
R48	o-xylene + Br = Product	1.6×10^{-14}	4
R49	m-xylene + Br = Product	7.9×10^{-14}	4
R50	p-xylene + Br = Product	4.0×10^{-14}	4
R51	α-pinene + Br = Product	6.8×10^{-14}	5
R52	MACR + Br = Product	3.9×10^{-10}	5
R53	MVK + Br = Product	2.3×10^{-10}	5
R54	MEK + Br = Product	3.6×10^{-10}	5
R55	ETOH + Br = Product	$8.6 \times 10^{-11}e^{45/T}$	5
R56	MEOH + Br = Product	5.5×10^{-11}	5
R57	$Cl + BrCl = Br + Cl_2$	1.45×10^{-11}	6
R58	$Cl + Br_2 = BrCl + Br$	1.94×10^{-10}	7

294   1. Sherwen et al. (2016); 2. Burkholder et al. (2020); 3. Keefer et al. (1950); 4. Giri et al. (2022); 5. Qinyi et al. (2021); 6. Clyne and Cruse.
295   (1972); 7.Khamaganov and Crowley. (2010)
296   MB3^a = CHBr$_3$, MB2^b = CH$_2$Br$_2$, MB2C^c = CH$_2$Br$_2$, MBC2^d = CHBr$_2$Cl, MBC^e = CH$_2$ClBr, FMBR^f = BrCHO

2.4.3 Iodine reactions

Iodine reactions taken into account in this study were acquired from Saiz-Lopez et al. (2014) and Sherwen et al. (2016). We updated iodine reactions in three ways: (i) updated absorption cross-sections for ICl and IBr (refer to R43 and R44 in Table 5); (ii) two inter-halogen species reactions (refer to R45 and R46 in Table 5); and (iii) nine heterogeneous reactions for $IONO_2$, INO_2, HOI, I_2O_2, I_2O_3, and I_2O_4 (refer to R11 to R19 in Table 3). These iodine reactions are shown in Tables 3 and 5.

304 **Table 5.** List of homogeneous iodine reactions used in this study.

No	Reaction	Reaction rate	Reference
R1	$I_2 \xrightarrow{h\nu} 2I$	#1.0/<I_2>	1
R2	$HOI \xrightarrow{h\nu} I + OH$	#1.0/<HOI>	1
R3	$IO \xrightarrow{h\nu} I + O^3P$	#1.0/<IO>	1
R4	$OIO \xrightarrow{h\nu} I$	#1.0/<OIO>	1
R5	$INO \xrightarrow{h\nu} I + NO$	#1.0/<INO>	1
R6	$INO_2 \xrightarrow{h\nu} I + NO_2$	#1.0/<INO_2>	1
R7	$IONO_2 \xrightarrow{h\nu} I + NO_3$	#1.0/<$IONO_2$>	1
R8	$I_2O_2 \xrightarrow{h\nu} I + OIO$	#1.0/<$IONO_2$>	1
R9	$I_2O_3 \xrightarrow{h\nu} IO + OIO$	#1.0/<$IONO_2$>	1
R10	$I_2O_4 \xrightarrow{h\nu} 2OIO$	#1.0/<$IONO_2$>	1
R11	$CH_3I \xrightarrow{h\nu} I + MEO2$	#1.0/<CH_3I>	1
R12	$MIC \xrightarrow{h\nu} I + Cl$	#1.0/<MIC>	1
R13	$MIB \xrightarrow{h\nu} I + Br$	#1.0/<INO_2>	1
R14	$MI2 \xrightarrow{h\nu} 2I$	#1.0/<$IONO_2$>	1
R15	$I + O_3 = IO$	$2.1 \times 10^{-11}e^{-830/T}$	2
R16	$I + HO_2 = HI$	$1.5 \times 10^{-11}e^{-1090/T}$	2
R17	$I_2 + OH = HOI + I$	2.1×10^{-10}	2
R18	$HI + OH = I$	$1.6 \times 10^{-11}e^{440/T}$	2
R19	$HOI + OH = IO$	5.0×10^{-12}	2
R20	$IO + HO_2 = HOI$	$1.4 \times 10^{-11}e^{540/T}$	2
R21	$IO + NO = I + NO_2$	$7.15 \times 10^{-12}e^{300/T}$	2
R22	$INO + INO = I_2 + 2NO$	$8.4 \times 10^{-11}e^{-2620/T}$	2
R23	$INO_2 + INO_2 = I_2 + NO_2$	$4.7 \times 10^{-13}e^{-1670/T}$	2
R24	$I_2 + NO_3 = I + IONO_2$	1.5×10^{-12}	2
R25	$IONO_2 + I = I_2 + NO_3$	$9.1 \times 10^{-11}e^{-146/T}$	2
R26	$I + BrO = IO + Br$	1.2×10^{-11}	2
R27	$IO + Br = I + BrO$	2.7×10^{-11}	2
R28	$IO + BrO = Br + I$	$1.5 \times 10^{-11}e^{510/T}$	2
R29	$IO + ClO = I + Cl$	$4.7 \times 10^{-12}e^{280/T}$	2
R30	$OIO + OIO = I_2O_4$	1.5×10^{-10}	2
R31	$OIO + NO = IO + NO_2$	$1.1 \times 10^{-12}e^{542/T}$	2
R32	$IO + IO = 0.4OIO + 0.4I + 0.6I_2O_2$	$5.4 \times 10^{-11}e^{180/T}$	2
R33	$IO + OIO = I_2O_3$	1.5×10^{-10}	2
R34	$I_2O_2 = OIO + I$	$2.5 \times 10^{-14}e^{-9770/T}$	2
R35	$I_2O_4 = 2OIO$	3.8×10^{-2}	2
R36	$INO_2 = NO_2 + I$	$9.9 \times 10^{17}e^{-11859/T}$	2
R37	$IONO_2 = NO_2 + IO$	$2.1 \times 10^{15}e^{-13670/T}$	2
R38	$CH_3I + OH = HCHO$	$4.3 \times 10^{-12}e^{-1120/T}$	2
R39	$IO + DMS = 0.75SO_2 + 0.25MSA + MEO2$	$3.3 \times 10^{-13}e^{-925/T}$	2
R40	$I + NO = INO$	1.8e-32^-1.0&1.7e-11^0.0&0.6&1.0	2
R41	$I + NO_2 = INO_2$	3.0e-31^-1.0&6.6e-11^0.0&0.6&1.0	2
R42	$IO + NO_2 = IONO_2$	7.7e-31^-3.5&7.7e-12^-.1.5&0.6&1.0	2
R43	$ICl \xrightarrow{h\nu} I + Cl$	#1.0/<ICl>	3
R44	$IBr \xrightarrow{h\nu} I + Br$	#1.0/<IBr>	3
R45	$Cl + I_2 = ICl + I$	2.81×10^{-10}	4
R46	$Br + I_2 = IBr + I$	1.2×10^{-10}	5

305 1. Sherwen et al. (2016); 2. Saiz-Lopez et al. (2014); 3. Burkholder et al. (2020); 4. Baklanov et al. (1997);
306 5.Bedjanian et al. (1997)
307

308 **2.5 Experimental design**

309   To better understand the impacts of atmospheric halogen chemistry, we designed four

310 experiments: (i) experiment without halogen chemistry (referred to as CTRL); (ii) original

311 CMAQv5.2.1 model simulation only with chlorine processes (EXP_{Cl}); (iii) experiment with

312 both chlorine and bromine processes (EXP_{Cl_Br}); and (iv) experiment with full halogen

313 processes ($EXP_{Cl\_Br\_I}$). The design of these four experiments is explained in Table 6.

314   In addition, in order to further analyze our results, we carried out two more

315 experiments: (i) CMAQ model runs with the halogen chemistry constructed by Saiz-Lopez et

316 al. (2014) (labeled as EXP_{CAM}); and (ii) CMAQ model run with the halogen chemistry

317 constructed by Sarwar et al. (2015) (labeled as EXP_{CMAQ}). The former halogen chemistry was

318 included in a global CTM named CAM-Chem, while the latter was in the CMAQ model. That

319 is why we labeled these two experiments, EXP_{CAM} and EXP_{CMAQ}, respectively.

320

321 **Table 6.** Description of the four experiments conducted in this study.

Experiment	Chlorine		Bromine		Iodine	
	Emission	Reaction	Emission	Reaction	Emission	Reaction
CTRL	-	-	-	-	-	-
EXP_{Cl}	√	√	-	-	-	-
EXP_{Cl_Br}	√	√	√	√	-	-
$EXP_{Cl\_Br\_I}$	√	√	√	√	√	√

322

323 **3. Results & Discussions**

324   In this section, we discuss the accuracy of new halogen chemistry and processes

325 through the comparison between simulated and measured mixing ratios of halogen-containing

326 compounds during the period of KORUS-AQ campaign. We then analyze the experimental

327 results to evaluate the impacts of atmospheric halogen chemistry and processes on key-species

328 concentrations in the atmosphere.

3.1 Model performances

3.1.1 Observed vs Modeled ClNO$_2$ mixing ratios

331   To evaluate the model performances, we used the mixing ratios of ClNO$_2$ observed at

332 two supersites (Olympic Park and Mt. Taehwa stations) in South Korea. Although the mixing

333 ratios of atmospheric Cl$_2$ were also measured at these two stations, we focused solely on ClNO$_2$

334 observations due to several uncertainties associated with Cl$_2$ analysis. These issues will be

335 discussed later in Sect. 3.1.3.

336   Figure 2 presents the diurnal variations of modeled and observed mixing ratios of

337 ClNO$_2$ at two monitoring stations. The CTRL simulation (black circles and lines in Fig. 2) and

338 EXP$_{CAM}$ (purple circles and lines in Fig. 2) could not reproduce the observed mixing ratios of

339 ClNO$_2$ at the two supersites. For instance, the average mixing ratios of ClNO$_2$ at both

340 monitoring stations were 0.00 ppt for CTRL and 15.40 ppt for EXP$_{CAM}$, while the observed

341 average mixing ratio of ClNO$_2$ was 122.67 ppt. This large discrepancy may be primarily due

342 to the absence of heterogeneous ClNO$_2$ formation via N$_2$O$_5$ in the halogen scheme

343 implemented for EXP$_{CAM}$, which was based on Saiz-Lopez et al. (2014). It is noted that this

344 mechanism was originally designed for clean, oceanic environments and does not account for

345 anthropogenic chlorine sources or inland ClNO$_2$ formation pathways, such as the reactions of

346 N$_2$O$_5$ with particulate chloride (recall R8: N$_2$O$_5$ + (1-φ) H$_2$O + η Cl$^-$ → (2-φ) HNO$_3$ +

347 φClNO$_2$). To address these limitations, recent versions of the model have incorporated the

348 previously missing pathways for HCl and ClNO$_2$ production (Li et al. 2022).

349   On the other hand, the EXP$_{CMAQ}$ (blue circles and lines in Fig. 2) and EXP$_{Cl\_Br\_I}$ (red

350 circles and lines in Fig. 2), which accounted for halogen chemistry, tend to better capture the

351 diurnal patterns of observed mixing ratios of ClNO$_2$ (refer to open circles and lines in Fig. 2).

352   These models also demonstrated significant improvements, in terms of statistical metrics

353   (which will be presented in Table 7).

354   Although the EXP_{CMAQ} showed reasonable agreement, it also exhibited significant

355   biases during the nighttime. Conversely, the $EXP_{Cl\_Br\_I}$ simulation achieved better agreement

356   with the observed mixing ratios of $ClNO_2$ at both stations. For example, the index of agreement

357   (IOA) increased from 0.62 for EXP_{CMAQ} to 0.66 for $EXP_{Cl\_Br\_I}$ and from 0.57 to 0.59 at

358   Olympic Park and Mt. Taehwa stations, respectively. These enhancements suggest that

359   successful implementation of the models depends on not only considering chlorine reactions

360   but also incorporating more comprehensive halogen reactions, as demonstrated by $EXP_{Cl\_Br\_I}$.

361   The following sections will explore and discuss these halogen reactions in the atmosphere.

362
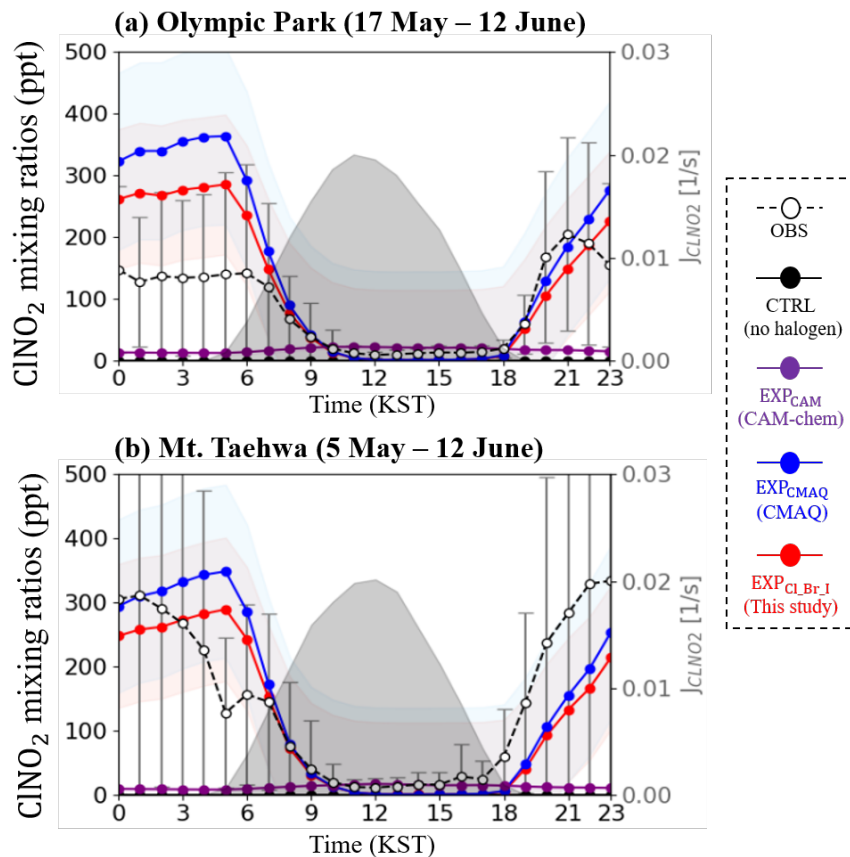
Figure 2. Diurnal variations in the mixing ratios of $ClNO_2$ (unit: ppt) at (a) Olympic Park and
(b) Mt.Taehwa stations during the period of the KORUS-AQ campaign. Observed values are
represented by open circles (error bars indicate the standard deviation). Colored lines with
shaded areas show the hourly-averaged mixing ratios of $ClNO_2$ and the corresponding standard

367 deviation from each simulation. The black shaded area indicates the variations in the photolysis
368 rate of $ClNO_2$ derived from the $EXP_{Cl\_Br\_I}$ simulation.
369
370
371 **Table 7.** Statistical metrics for $ClNO_2$ analysis from CTRL, EXP_{CAM}, EXP_{CMAQ}, and $EXP_{Cl\_Br\_I}$
372 simulations at the Olympic Park and Mt.Taewha stations during the period of KORUS-AQ
373 campaign.

Target: $ClNO_2$		Olympic Park	Mt.Taehwa
	Observed mean (ppt)	85.97	159.36
CTRL	Modeled mean (ppt)	0	0
	MB (ppt)	-85.97	-159.36
	RMSE (ppt)	150.30	288.82
	IOA	0.41	0.40
EXP_{CAM}	Modeled mean (ppt)	17.31	13.49
	MB (ppt)	-68.67	-145.87
	RMSE (ppt)	143.23	281.78
	IOA	0.37	0.40
EXP_{CMAQ}	Modeled mean (ppt)	135.77	152.89
	MB (ppt)	49.80	-6.65
	RMSE (ppt)	204.42	289.19
	IOA	0.62	0.57
$EXP_{Cl\_Br\_I}$	Modeled mean (ppt)	116.76	134.29
	MB (ppt)	30.79	-25.07
	RMSE (ppt)	174.41	272.69
	IOA	0.66	0.59

374

3.1.2 Contributions to mixing ratios of $ClNO_2$

376 Figure 3a and 3c represent the diurnal variations in the mixing ratios of $ClNO_2$ from

377 the EXP_{CMAQ} (blue dotted line) and $EXP_{Cl\_Br\_I}$ simulations (red dotted line) at two supersites

378 during the period of the KORUS-AQ campaign. Through a sensitivity test, we attempted to

379 identify the key reactions in the $EXP_{Cl\_Br\_I}$ causing differences from the EXP_{CMAQ} simulation.

380 From the studies, we identified four critical halogen reactions: (i) updated reaction rate

381 coefficient of R20 in Table 1; (ii) newly added heterogeneous reaction of HOBr as shown in

382 R8 of Table 3; (iii) modified parameterization of γ_{N2O5} as shown in R1 of Table 3; and (iv)

383 newly added heterogeneous reaction of NO_2 onto atmospheric aerosols as shown in R6 of Table

384 3. The contributions of these four reactions were calculated and are presented in blue-, green-,

385 yellow-, and red-shaded areas in Fig. 3, respectively. It is evident that the contribution of the

386 parameterization of γ_{N2O5} is the most significant. A detailed analysis of these differences

387 between EXP$_{CMAQ}$ and the EXP$_{Cl\_Br\_I}$ is further discussed in Table S2.

388   Figure 3b and 3d illustrate the contributions of the four reactions to the mixing ratios

389 of ClNO$_2$ at the two supersites. Our results again indicate that selecting the new γ_{N2O5} led to

390 the largest decreases in the averaged mixing ratios of ClNO$_2$ by 9.58 ppt (50.4%) and 7.50 ppt

391 (40.3%) at the Olympic Park and Mt. Taehwa stations, respectively. These reductions are

392 obviously attributed to lower values of γ_{N2O5} in EXP$_{Cl\_Br\_I}$ (γ_{N2O5} = ~0.013), compared to

393 those in EXP$_{CMAQ}$ (γ_{N2O5} = ~0.014) as shown in Fig. S3. Such a small difference in γ_{N2O5}

394 led to substantial differences in the mixing ratios of ClNO$_2$. In addition, the inclusion of

395 reaction (recall R20: ClO + ClO → Cl$_2$), with its rate constant reduced by a factor of 10 from

396 the original CMAQ model (see Table S2), led to a 3.40 ppt (17.8%) decrease in the ClNO$_2$

397 mixing ratio at the Olympic Park station. This effect is likely due to the slower removal of ClO,

398 which resulted in slightly elevated ClO levels in the boundary layer. The increased ClO may

399 have promoted the formation of ClONO$_2$ (i.e., reservoir species) via reaction with NO$_2$, thereby

400 reducing the amount of reactive nitrogen available for ClNO$_2$ production through the

401 heterogeneous pathway. Accounting for the heterogeneous reaction of NO$_2$ and HOBr onto

402 chlorine-containing particles also resulted in reductions in the mixing ratios of ClNO$_2$ by 4.46

403 ppt (24.0%) and 2.77 ppt (14.9%) at the Mt. Taehwa station, respectively. These reactions

404 competitively consume chloride-containing particles, thereby reducing the availability of

405 particulate chlorine that is essential for ClNO$_2$ formation. Overall, these results indicate that

406 the reduction in the ClNO$_2$ mixing ratios was primarily driven by the updated chlorine

407 chemistry, particularly the revised parameterization of γ_{N2O5} and the inclusion of additional

408 chlorine-related reactions, with secondary contributions from bromine chemistry.

409   Collectively, the four reactions mentioned above may be the key reactions that can

410 significantly change the atmospheric levels of ClNO$_2$. Nevertheless, it should also be noted

that the $EXP_{Cl\_Br\_I}$ simulation still exhibited discrepancies with the observed mixing ratios of

$ClNO_2$. These remaining biases may be attributed to factors not fully accounted for in the

current modeling framework, including (i) the uptake of Cl_2 or related species onto aerosol

surfaces, (ii) uncertainties in the $ClNO_2$ yield, (iii) simplified diurnal emissions profiles for

HCl and Cl_2, and (iv) missing constrained halogen reactions. These limitations require further

targeted sensitivity analyses to better quantify their individual and combined impacts.
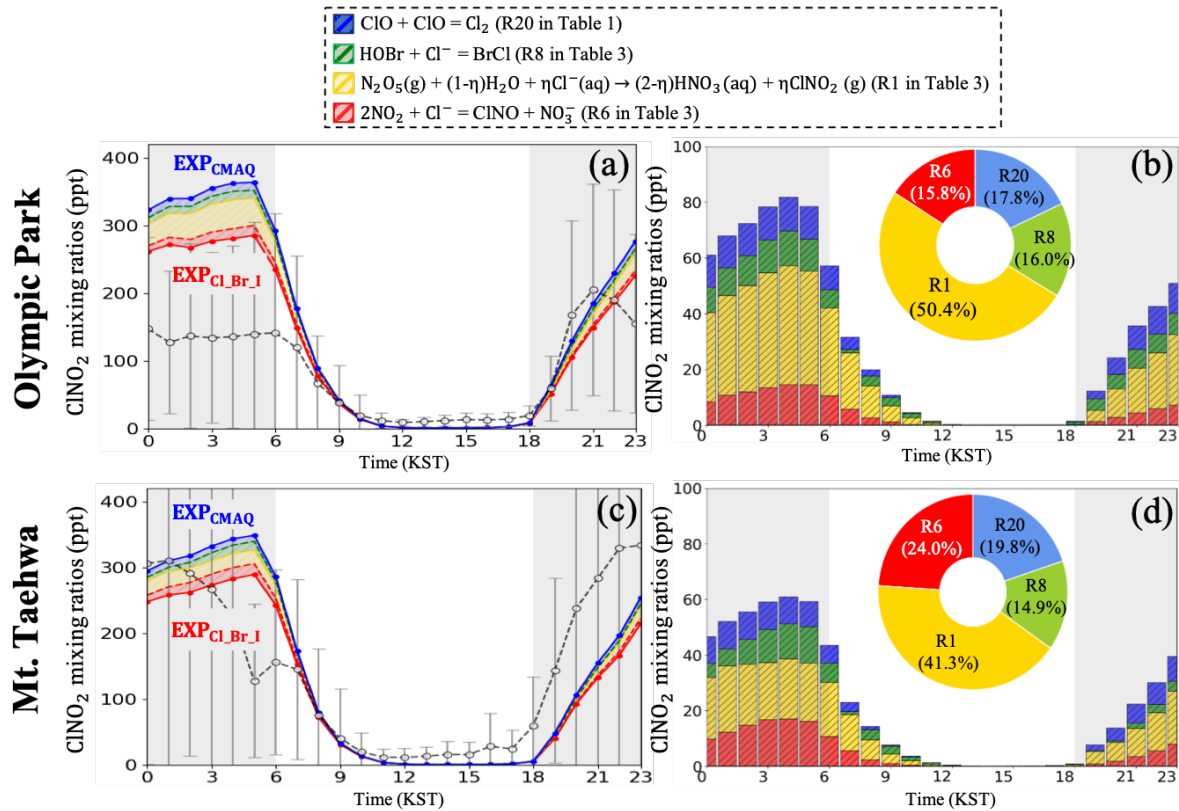
Figure 3. Contributions of halogen reactions to the mixing ratios of $ClNO_2$ in the EXP_{CMAQ}
and $EXP_{Cl\_Br\_I}$ simulations at (a and b) Olympic Park and (c and d) Mt. Taehwa stations during
the period of KORUS-AQ campaign. Stacked bars and pie charts show the contributions from
four halogen reactions to the mixing ratios of $ClNO_2$. Grey-shaded areas represent nighttime
(18:00-06:00 local standard time).

3.1.3 Uncertainties in Cl_2

Figure 4 represents bar graphs of 24-hour averaged Cl_2 mixing ratios from the four

experiments, together with the observed Cl_2 mixing ratios at two supersites. Among them, the

mixing ratios of Cl_2 from the $EXP_{Cl\_Br\_I}$ agree well with the observed mixing ratios of Cl_2.

428 Based on these findings, we attempted to analyze which reactions contributed to elevated levels

429 of Cl_2. Two key reactions were identified: (i) $HOCl + Cl^- \rightarrow Cl_2$ (R2 in Table 3) and (ii)

430 $ClONO_2 + Cl^- \rightarrow Cl_2$ (R3 in Table 3). These reactions accounted for an increase in Cl_2 of

431 0.18 ppt (14.2%) and 1.06 ppt (84.1%), respectively, at the two supersites.

432 Although the current modeling system has improved the predictions of 'campaign-

433 averaged' Cl_2 mixing ratios, it has a serious limitation in reproducing daytime Cl_2 levels, likely

434 due to the extremely fast photo-dissociation rate of Cl_2 (J_{Cl2} is estimated at 2.5×10^{-3} s^{-1}). In

435 other words, once Cl_2 was produced via daytime halogen reaction pathways (see R3 to R5 in

436 Table 3), it was rapidly removed by the fast photo-dissociation. To address this challenge,

437 several studies suggested potential missing daytime reactions, such as particulate nitrate

438 photolysis and the uptake of O_3 and OH onto atmospheric particles (Peng et al., 2022; Chen et

439 al., 2022). However, these reactions also have limitations in perfectly explaining the relatively

440 high levels of Cl_2 during the daytime. Although the model slightly overestimates Cl_2 mixing

441 ratios during the nighttime (by approximately 0.3 ppt), the major discrepancy lies in the

442 inability to capture daytime peaks. In this context, the accuracy of simulating daytime Cl_2

443 mixing ratios remains a topic of further discussion.

444 In addition, significant uncertainties have been reported in observing Cl_2 mixing ratios

445 using the CIMS instrument. The detection limit for Cl_2 in the CIMS instrument was estimated

446 to be 2.9 ppt over a 30-minute interval (Jeong et al., 2019). However, the averaged mixing

447 ratios of Cl_2 of 2.08 ppt and 2.69 ppt were measured at Olympic Park and Mt. Taehwa,

448 respectively, as depicted in Fig. 4. Given that the observed levels of Cl_2 at the two monitoring

449 stations were very close to the detection limit of the instrument, significant uncertainties likely

450 exist in these measurements of the mixing ratios of Cl_2.
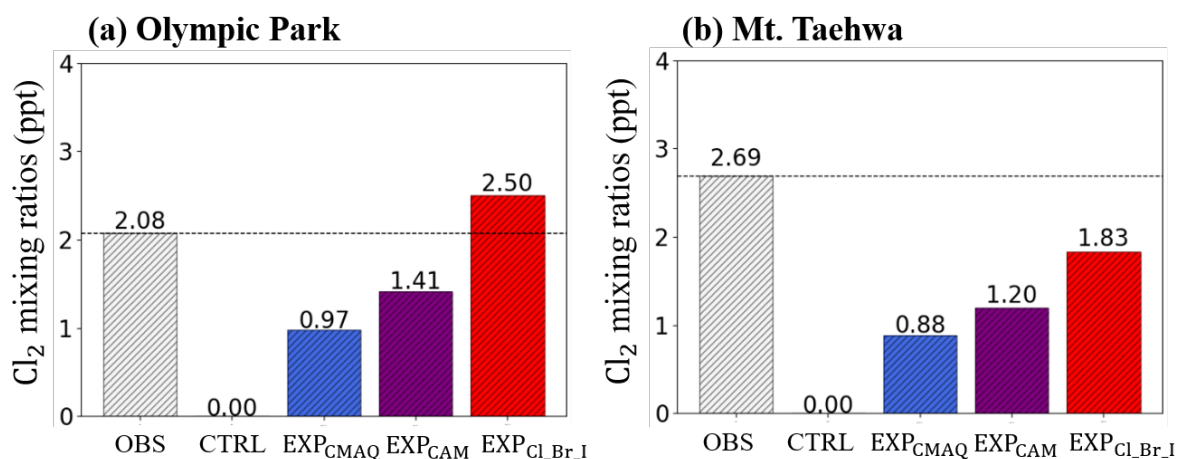
Figure 4. Comparisons of averaged mixing ratios of Cl_2 observed (OBS) and modeled from four simulations (CTRL, EXP_{CMAQ}, EXP_{CAM}, and $EXP_{Cl\_Br\_I}$) at (a) Olympic Park and (b) Mt. Taehwa stations. Dotted lines represent the observed mixing ratios of Cl_2.

3.1.4 Levels of bromine monoxide (BrO) and iodine monoxide (IO)

To strengthen the model evaluation, we also compared simulated bromine monoxide (BrO) and iodine monoxide (IO) levels with previously reported observational and modeling data, as shown in Fig. 5.

As illustrated in Fig. 5a, several modeling studies reported the mixing ratios of BrO ranging from 0.0 to 1.3 ppt (Koenig et al., 2017; Le Breton et al., 2017; Fan and Li, 2022; Zhu et al., 2019; Li et al., 2020; Li et al., 2019), which are similar to observed values (Koenig et al., 2017; Peters et al., 2005). Our simulation results indicate relatively low BrO mixing ratios, which may be attributed to low levels of chlorophyll-a over the Korean Peninsula during May and June (Son, 2013).

For IO, previous field and modeling studies have reported the mixing ratios of IO ranging from 0.0 to 2.5 ppt (Großmann et al., 2013; Allan et al., 2000; Fan and Li, 2022; Li et al., 2020; Takashima et al., 2021; Prados-Román et al., 2015; Mahajan et al., 2012; Mahajan et al., 2010; Inamdar et al., 2020). Overall, our simulated IO mixing ratios (0.0 – 1.8 ppt) over

471 the East Asian ocean region during the KORUS-AQ campaign is comparable to previously

472 reported ranges, as shown in Fig. 5b.

473   Although BrO and IO were not directly measured during the KORUS-AQ campaign,

474 this comparison suggests that our simulated halogen species are within a reasonable range of

475 previously reported values. These indirect evaluations complement the $ClNO_2$-based validation

476 and enhance confidence in our model's ability to simulate regional-scale behavior of bromine

477 and iodine species.

478
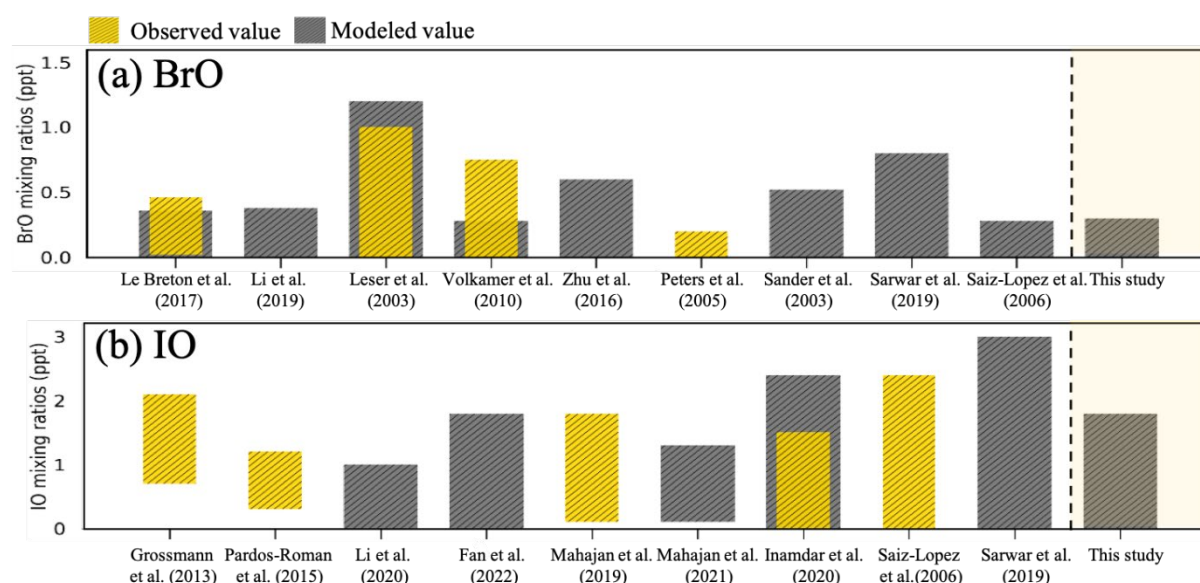
479 **Figure 5.** Comparisons between modeled and observed mixing ratios of atmospheric (a) BrO
480 and (b) IO. Both are observed and modeled mixing ratios were obtained from the previous
481 studies.

482

483 **3.2 Influences of halogen chemistry on O_3 mixing ratios**

484 **3.2.1 Comparative analysis at three supersites**

485   Based on the evaluation of model performances, we analyzed the impacts of halogen

486 processes on atmospheric O_3 mixing ratios at three monitoring stations (regarding the locations,

487 see Fig. 1a). Fig. 6 represents the diurnal variations in the mixing ratios of O_3 as simulated

488 from both the CTRL (black circles) and $EXP_{Cl\_Br\_I}$ (red circles), together with the observations

489   (white open circles) during the period of the KORUS-AQ campaign. It shows that the O_3

490   mixing ratios simulated from the $EXP_{Cl\_Br\_I}$ slightly increased by ~0.06 ppb (0.3%) and ~0.14

491   ppb (0.4%), higher than those from the CTRL at Olympic Park and Mt. Taehwa stations,

492   respectively. Similar patterns were also observed in the comparisons between O_3 observations

493   from 320 AIR-KOREA stations and O_3 predictions (as shown in Fig. S4).

494   It should be noted that the simulated O_3 mixing ratios decreased slightly by ~0.19 ppb

495   (0.3%), lower than those simulated from the CTRL at the Bangnyung station. These results

496   raised two questions: (i) why did the opposite patterns take place between two land stations

497   and one ocean station (Bangnyung Island station)? and (ii) what mechanism caused these

498   opposite patterns in the mixing ratios of O_3? To answer these two questions, we further

499   investigated the role of halogen chemistry in atmospheric O_3 chemistry.

500
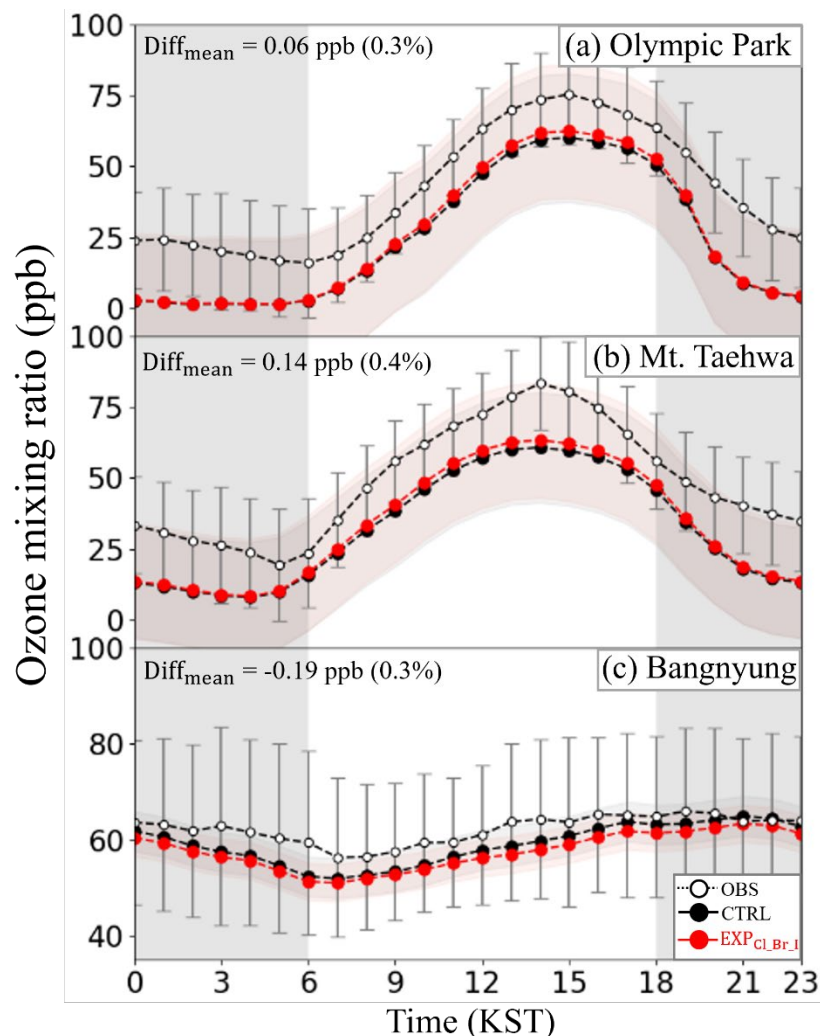
Figure 6. Diurnal variations in the mixing ratios of O_3 from CTRL (black circles) and $EXP_{CL\_Br\_I}$ (red circles) simulations, together with observed mixing ratios of O_3 (OBS; white circles) at (a) Olympic Park, (b) Mt. Taehwa, and (c) Bangnyung stations during the period of the KORUS-AQ campaign. Error bars and shaded areas indicate the standard deviations of observed and modeled O_3, while the grey-shaded areas show the nighttime. $DIFF_{mean}$ represents the difference in the averaged mixing ratios of O_3 between $EXP_{Cl\_Br\_I}$ and CTRL simulations.

3.2.2 Impacts of halogen processes

Figure 7 illustrates the spatial distributions of the differences between two O_3 mixing ratios simulated under the consideration of individual halogen chemistry over the Korean peninsula. The CMAQ-simulated O_3 mixing ratios for EXP_{Cl} showed an increase of 0.62 ppb (1.4%) compared to those from the CTRL over the Korean peninsula (as shown in Fig. 7a).

513   This increase is attributed to the VOC oxidation by Cl radicals, which leads to the production

514   of additional RO_2 radicals. Additional O_3 is subsequently produced via the $RO_2 + NO$ reactions.

515   It is well-known that VOC oxidation rates by Cl radicals are approximately 10 times faster than

516   those by OH radicals (Edwards and Young, 2024). Several previous studies have also

517   confirmed these findings (Kim et al., 2023; Jo et al., 2023).

518   Bromine-containing species are known to contribute to O_3 destruction in the

519   atmosphere. However, VOC oxidations by Br radicals also contribute to atmospheric O_3

520   formation via the reactions of $Br + VOC \rightarrow$ products $+ RO_2$ (these reactions are shown in R36

521   to R57 in Table 4). As a result, the net effects of bromine processes (i.e., $EXP_{Cl\_Br} - EXP_{Cl}$)

522   lead to a slight increase in O_3 mixing ratios of ~0.01 ppb, as shown in Fig. 7b. This negligible

523   increase is likely due to the competition between O_3 loss via bromine-catalyzed destruction

524   and O_3 production via VOC oxidation.

525   In Fig. 7c, when iodine processes were incorporated into the modeling system, the

526   surface-averaged O_3 mixing ratios decreased by ~1.39 ppb (2.4%), particularly over ocean

527   areas. The iodine radicals generated from the photolysis of marine-originated iodine species

528   primarily react with O_3. Given the low levels of VOCs over ocean areas, iodine radicals

529   predominantly participate in the O_3 destruction over the ocean.

530   Again, the O_3 mixing ratios are controlled by competition between the O_3 production

531   and O_3 destruction. We found that the average O_3 mixing ratios increased by 0.21 ppb (~0.5%)

532   over land areas and decreased by 0.69 ppb (~1.2%) over ocean areas under the considerations

533   of entire halogen processes (i.e., $EXP_{Cl\_Br\_I} - CTRL$) (refer to Figs. 7d and S5). These findings

534   are closely in line with the increases in O_3 mixing ratios at the Olympic Park and Mt. Taehwa

535   stations (located on land areas) and the decreases in O_3 mixing ratios at the Bangnyung station

536   (located around ocean areas) under the comprehensive considerations of the halogen chemistry,

537   as discussed in Sect. 3.2.1. Such contrasting effects of halogen chemistry between polluted

538 continental and pristine oceanic regions are consistent with previous studies (e.g., Li et al.,

539 2022; Saiz-Lopez et al., 2023), which have also reported O_3 enhancements over land and

540 reductions over the ocean.

541
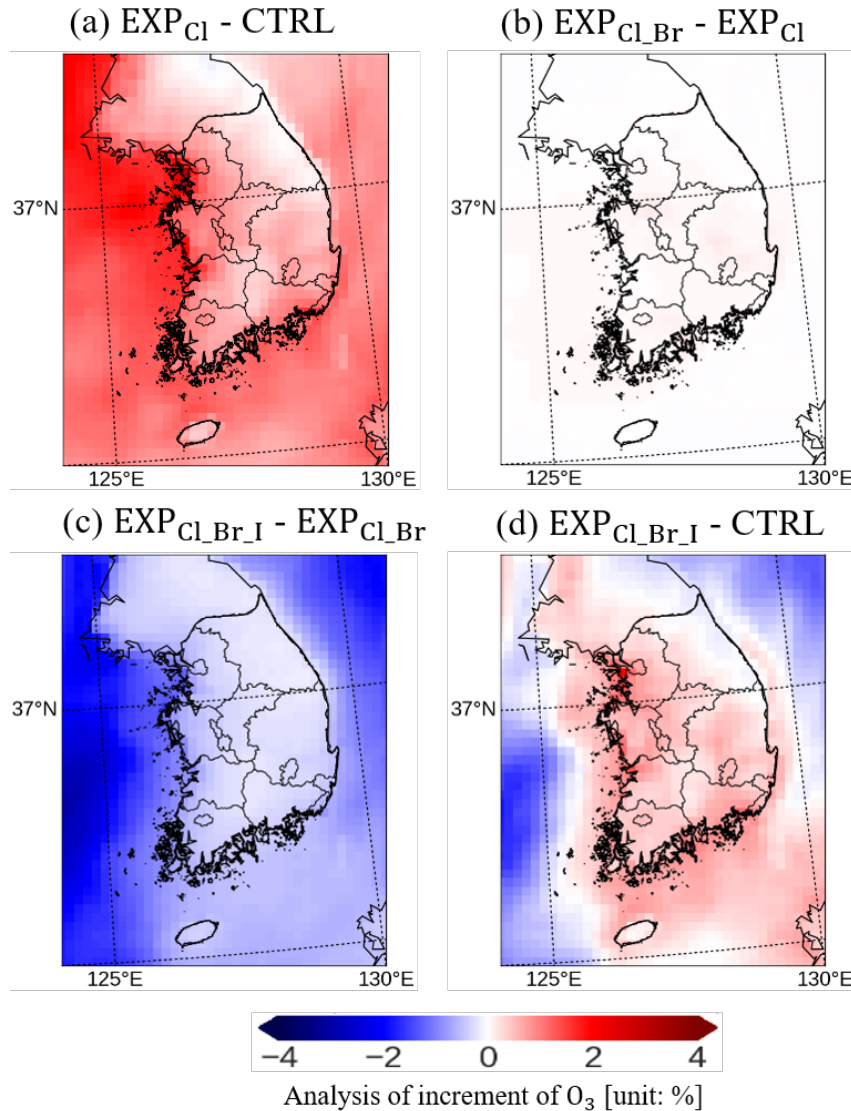
542 **Figure 7.** Spatial impacts of (a) chlorine processes (EXP_{Cl} - CTRL), (b) bromine processes
543 (EXP_{Cl_Br} − EXP_{Cl}), (c) iodine processes ($EXP_{Cl\_Br\_I}$ − EXP_{Cl_Br}), and (d) total halogen
544 processes ($EXP_{Cl\_Br\_I}$ − CTRL) on O_3 mixing ratios over the Korean peninsula.
545

546 **3.2.3 Net O_x production**

547   To better understand the influences of the halogen chemistry on atmospheric O_3 mixing

548 ratios, we additionally carried out a quantitative analysis. We calculated O_x production rates

549    $(P(O_x))$ utilizing a definition of expanded O_x family ($\equiv O_3 + O^{1D} + O^{3p} + NO_2 + 2NO_3 +$

550    $3N_2O_5 + XNO_2 + XO + XONO_2$; here, X denotes Cl, Br, and I). The constructions of the $P(O_x)$

551   are shown in equations (8) to (10):

552    $$F(O_x) = k_{HO_2+NO}[HO_2][NO] + k_{RO_2+NO}[RO_2][NO] \qquad \text{(Eq. 8)}$$

553    $$D(O_x) = k_{NO_2+OH}[NO_2][OH] + k_{O_3+VOC}[O_3][VOC] + k_{O(1D)+H_2O}[O(^1D)][H_2O]$$

554    $$+ k_{O_3+OH}[O_3][OH] + k_{O_3+HO_2}[O_3][HO_2] + k_{RO_2+NO_2}[RO_2][NO_2]$$

555    $$+ (k_{XO+O_3}[O_3] + k_{XO+HO_2}[HO_2] + k_{XO+O(3p)}[O(^3P)])[XO]$$

556    $$+ k_{ClO+NO_2}[NO_2][ClO] + k_{XO+XO}[XO]^2 + k_{NO_3+VOC}[NO_3][VOC]$$

557    $$+ 3k_{het}[N_2O_5] \qquad \text{(Eq. 9)}$$

558    $$P(O_x) = F(O_x) - D(O_x) \qquad \text{(Eq. 10)}$$

559   where $F(O_x)$ and $D(O_x)$ represent the O_x formation rates and O_x destruction rates, respectively.

560   k_i and k_{het} denote the reaction rate constants for reaction i and heterogeneous reactions of N_2O_5,

561   respectively.

562   Figure 8 shows the average O_x formation rates ($F(O_x)$), O_x destruction rates ($D(O_x)$),

563   and the $P(O_x)$ from the CTRL and $EXP_{Cl\_Br\_I}$ simulations. Over land, rates for reactions of RO_2

564   + NO and HO_2 + NO in the $F(O_x)$ increased from 2.16 ppb/h to 2.21 ppb/h and from 2.05 ppb/h

565   to 2.09 ppb/h, respectively, with the full consideration of the halogen processes in the CMAQ

566   model. On the contrary, $D(O_x)$ decreased from 1.12 ppb/h to 0.97 ppb/h due to the limited

567   contribution of O_3 destruction by halogen radicals. Consequently, $P(O_x)$ increased from 3.08

568   ppb/h to 3.33 ppb/h. The enhanced $F(O_x)$ of 0.09 ppb/h with decreased $D(O_x)$ of 0.15 ppb/h

569   contributes to the increase in $P(O_x)$ of 0.25 ppb/h. Consistent results were observed at the

570   Olympic Park and Mt. Taehwa stations (as shown in Figs. 6a and 6b).

571   On the other hand, the $F(O_x)$ decreased by 0.03 ppb/h, while both $D(O_x)$ and $P(O_x)$

572   increased by 0.12 ppb/h and 0.14 ppb/h, respectively, over the ocean (refer to Fig. 8b and Table

573   8). This may be caused by the halogen-related losses in $D(O_x)$ (caused mainly by $IO + HO_2$

574   reaction), significantly contributing to the O_3 destruction. These results indicate that the mixing

575   ratios of O_3 tend to decrease in the presence of iodine radicals over the ocean areas. This is also

576   in line with the case of the Bangnyung station, shown in Fig. 6c.

577
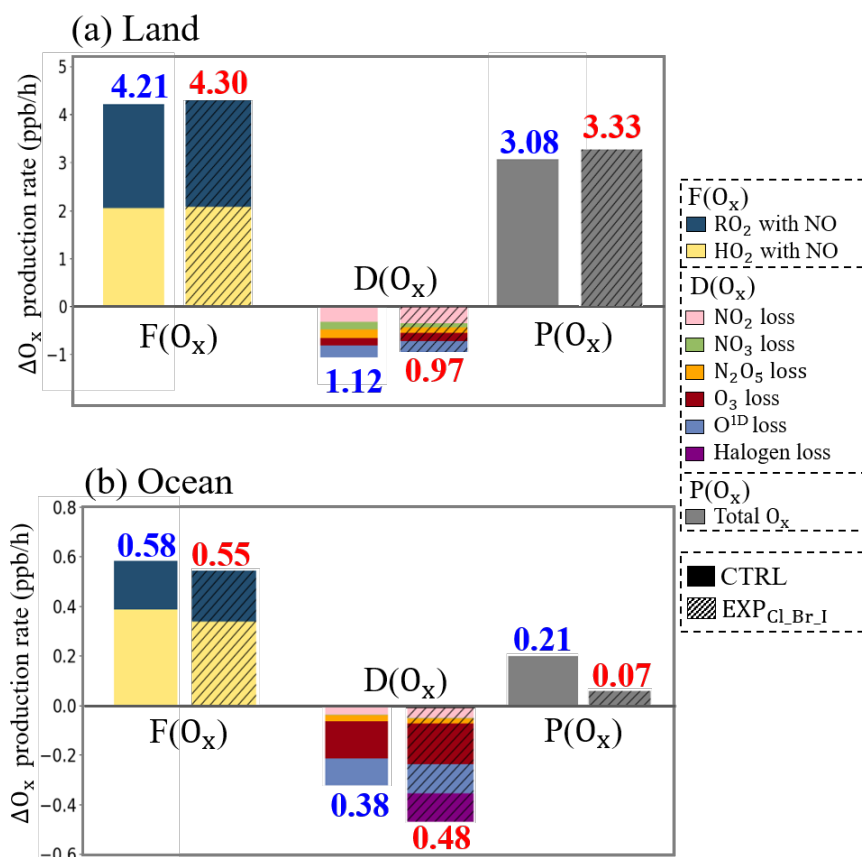
Figure 8. The stacked bar graphs represent O_x formation rate ($F(O_x)$), destruction rate ($D(Ox)$),
and production rate ($P(O_x)$) in the CTRL (plain bars) and $EXP_{Cl\_Br\_I}$ (hatched bars) simulations
over the (a) land and (b) ocean areas, respectively, during the period of KORUS-AQ campaign.
Individual reactions contributing to $F(O_x)$ and $D(O_x)$ are indicated by the bar colors.

Table 8. Averaged budget for O_x formation rates (F(O_x)), O_x destruction rates (D(O_x)), and O_x production rates (P(O_x)) calculated from the CTRL and EXP$_{Cl\_Br\_I}$ simulations during the period of KORUS-AQ campaign.

	Land		Ocean	
	CTRL	EXP$_{Cl\_Br\_I}$	CTRL	EXP$_{Cl\_Br\_I}$
O_x Formation: F(O_x)				
RO$_2$ + NO	2.16	2.21	0.20	0.21
HO$_2$ + NO	2.05	2.09	0.39	0.34
Total F(O_x)	4.21	4.30	0.58	0.55
O_x Destruction: D(O_x)				
NO$_2$ loss[1]	0.33	0.35	0.05	0.04
NO$_3$ loss[2]	0.17	0.09	< 0.01	< 0.01
N$_2$O$_5$ loss[3]	0.20	0.12	0.03	0.02
O$_3$ loss[4]	0.26	0.24	0.13	0.12
O^{1D} loss[5]	0.16	0.17	0.18	0.17
Halogen loss[6]	0	0.01	0	0.12
Total D(O_x)	1.12	0.97	0.38	0.48
Total O_x production: P(O_x)				
P(O_x) = F(O_x) - D(O_x)	3.08	3.33	0.21	0.07

NO$_2$ loss[1]= NO$_2$+RO$_2$ and NO$_2$+OH
NO$_3$ loss[2]= NO$_3$+VOC
N$_2$O$_5$ loss[3]= Heterogeneous reaction of N$_2$O$_5$
O$_3$ loss[4]= O$_3$ + OH, O$_3$ + VOC, and O$_3$ + HO$_2$
O^{1D} loss[5]= O^{1D}+H$_2$O
Halogen loss[6]= XO + O$_3$, HO$_2$, and O^{3p}; ClO + NO$_2$; XO + XO (where X denotes Cl, Br, and I)

3.3 Impacts of halogen chemistry on atmospheric species

Figure 9 summarizes the impacts of halogen processes on the mixing ratios of key atmospheric species over/around the Korean peninsula. The mixing ratios of hydroxyl radicals (OH) and hydroperoxyl radicals (HO$_2$) increased by ~0.002 ppt (2.2%) and ~0.13 ppt (1.6%), respectively, when including the chlorine processes (i.e., EXP$_{Cl}$ - CTRL). This is due to the fact that the chlorine radicals in the atmosphere substitute the role of OH radicals. In other words, chlorine radicals actively react with VOCs. Thus, the VOC mixing ratios decreased by 0.39 ppb (1.0%) due to the active VOC oxidation by Cl radicals. Formaldehyde (HCHO), an intermediate product of VOC oxidation, increased by 0.02 ppb (1.1%) due to the enhanced rates of the VOC oxidation by Cl radicals. The NO$_x$ mixing ratios also increased by ~0.26 ppb

603   (2.6%). Higher levels of NO_x may be due to the elevated levels of $ClNO_2$, which is a precursor

604   of NO_x in the atmosphere.

605   We also explored the impacts of bromine processes (i.e., $EXP_{Cl\_Br} - EXP_{Cl}$). The

606   mixing ratios of OH, HO_2, and HCHO further increased by ~0.001 ppt (1.1%), ~0.03 ppt (0.4%),

607   and ~0.01 ppb (0.5%), respectively. These patterns appear to be similar to those in the chlorine

608   case.

609   The effects of iodine chemistry (i.e., $EXP_{Cl\_Br\_I} - EXP_{Cl\_Br}$) revealed that OH mixing

610   ratios increased by 0.004 ppt (3.1%). However, the mixing ratios of HO_2 decreased by 0.32 ppt

611   (3.8%). Interestingly, this increase in OH contrasts with a previous global-scale study (e.g., Li

612   et al., 2022), where iodine chemistry typically leads to lower OH due to halogen-driven O_3

613   suppression and reduced $O(^1D)$ production. This discrepancy can likely be attributed to

614   differences in the spatial and temporal scales of the analysis. Specifically, our study focuses on

615   a short-term episode (i.e., the KORUS-AQ campaign), during which OH mixing ratios may be

616   more strongly influenced by halogen-mediated radical regeneration. For instance, reactions

617   such as $IO + HO_2 \rightarrow HOI$, followed by HOI photolysis ($HOI \overset{h\nu}{\rightarrow} I + OH$), can provide an

618   additional OH source that partially compensate for the O_3-related OH loss. Similar findings

619   have been reported in previous studies (Saiz-Lopez et al., 2012; Mahajan et al., 2021; Stone et

620   al., 2018). The levels of HCHO and VOCs remain almost unchanged due to the fact that iodine

621   radicals do not strongly participate in the reactions with VOCs. The NO_x levels increased

622   slightly by ~0.03 ppb (0.3%) on land and decreased by ~0.03 ppb (4.8%) over ocean areas,

623   which is in line with findings from the previous study (Mahajan et al., 2021).

624   Collectively, the influence of the full halogen chemistry (i.e., $EXP_{Cl\_Br\_I} - CTRL$)

625   shows that the OH mixing ratios increased significantly by 0.007 ppt (5.5%), while the HO_2

626   mixing ratios decreased by 0.45 ppt (5.3%) over ocean areas. These patterns are comparable in

627   magnitude to those reported in previous studies. For example, Stone et al. (2018) reported a 2%

628   increase in OH and a 5% decrease in HO_2, while Chen et al. (2024) found larger changes with

629   a 12% increase in OH and an 8% decrease in HO_2. In addition, Sarwar et al. (2015) found a

630   slight decrease in OH (1%) accompanied by a more pronounced decrease in HO_2 (11%). The

631   mixing ratios of HCHO and NO_x increased by ~0.03 ppb (1.6%) and ~0.29 ppb (2.9%) over

632   the land. On the contrary, the mixing ratios of VOCs and NO_x decreased by ~0.71 ppb (5.9%)

633   and ~0.05 ppb (7.8%) over the ocean areas, respectively. The reduction in NO_x over ocean is

634   consistent with Wang et al. (2021), who reported a similar decrease of approximately 6% due

635   to halogen chemistry.

636   In addition, elevated oxidant capacity in the simulation of $EXP_{Cl\_Br\_I}$ results in

637   enhancements in the concentrations of sulfate by 0.05 $\mu g \cdot m^{-3}$ (1.5%) and secondary organic

638   aerosols by 0.14 $\mu g \cdot m^{-3}$ (1.8%). However, concentrations of nitrate and ammonium decreased

639   by ~1.60 $\mu g \cdot m^{-3}$ (29.4%) and ~0.55 $\mu g \cdot m^{-3}$ (5.0%), respectively, as shown in Fig. S6. This

640   resulted from using smaller uptake coefficient for N_2O_5 (refer to Fig. S3), which suppresses

641   NH_4NO_3 formation. As a result, $PM_{2.5}$ levels decreased from 21.59 $\mu g \cdot m^{-3}$ to 20.63 $\mu g \cdot m^{-3}$

642   (10.5%) over the Korean Peninsula during the KORUS-AQ campaign.
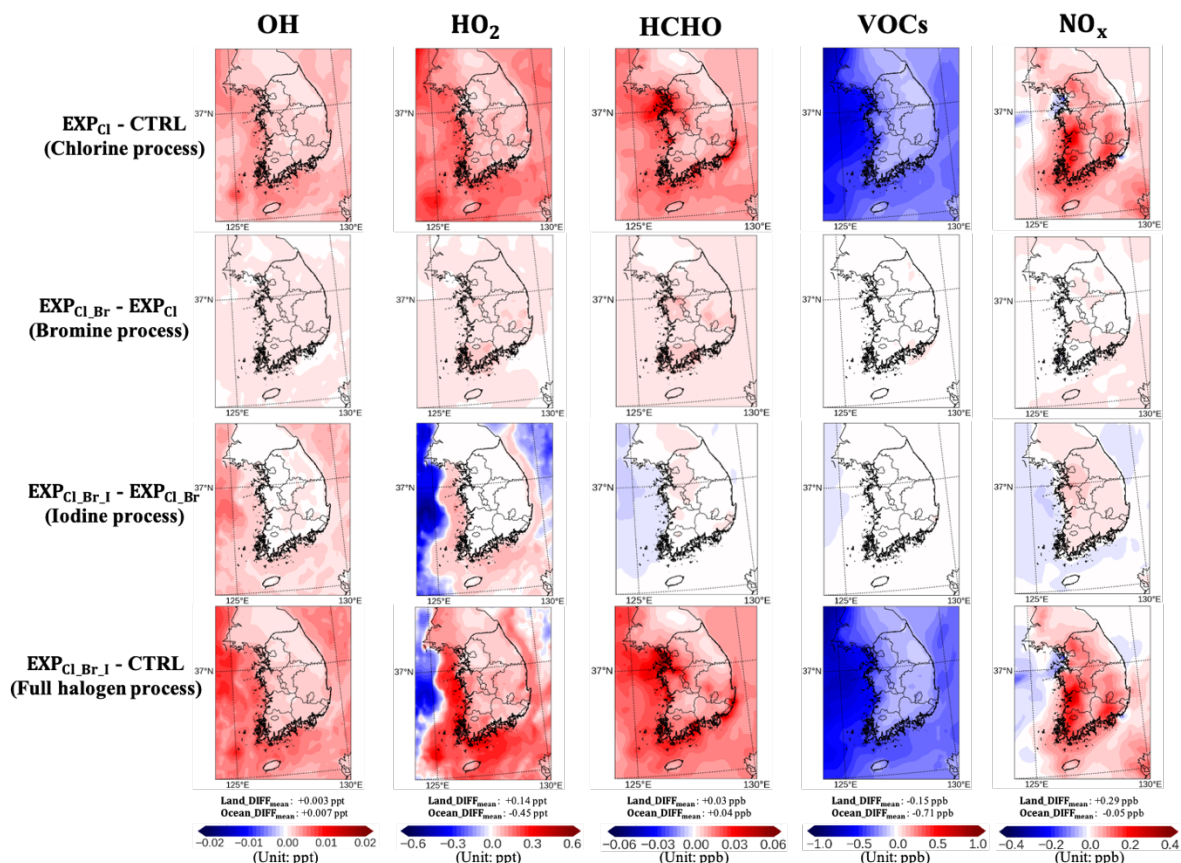
Figure 9. Summaries of the impacts of chlorine processes (EXP_{Cl} – CTRL), bromine processes (EXP_{Cl_Br} – EXP_{Cl}), iodine processes ($EXP_{Cl\_Br\_I}$ – EXP_{Cl_Br}), and full halogen processes ($EXP_{Cl\_Br\_I}$ – CTRL) on the mixing ratios of OH, HO_2, HCHO, VOCs, and NO_x, respectively, during the period of KORUS-AQ campaign. Also, Land_DIFF$_{mean}$ and Ocean_DIFF$_{mean}$ indicate the differences in the averaged mixing ratios of each species between $EXP_{Cl\_Br\_I}$ and CTRL simulations, over land and ocean, respectively.

4. Summary and Conclusions

To investigate the impacts of halogen chemistry over the Korean peninsula, we attempted to add and update reactions involving three halogen species (Cl, Br, and I) in the CMAQ modeling system. First, we estimated anthropogenic emissions of HCl, Cl_2, HBr, and Br_2 from five main sectors (such as industry, residential areas, power plants, solid waste incineration, and others). The anthropogenic emissions for HCl, Cl_2, HBr, and Br_2 were estimated to be 5,989.6, 450.8, 460.8, and 240.8 Mg·yr^{-1} over our research domain, respectively. Second, we also estimated emissions of natural halocarbons and inorganic bromine and iodine

659 (Br_2, I_2, and HOI), based on the information derived from the GOCI sensor. Finally, we

660 embedded halogen chemical reactions (58 chlorine reactions, 64 bromine reactions, and 55

661 iodine reactions) into the CMAQ model.

662   We then tested the model performances in terms of the mixing ratios of $ClNO_2$ during

663 the period of the KORUS-AQ campaign at two supersites in South Korea. The $EXP_{Cl\_Br\_I}$

664 simulation exhibited the best performance in terms of the mixing ratios of $ClNO_2$. With the

665 $EXP_{Cl\_Br\_I}$ simulation, the IOA increased from 0.41 to 0.66 at the Olympic Park station, and

666 0.40 to 0.59 at the Mt. Taehwa station. Meanwhile, the MB decreased from -85.97 ppt to 30.79

667 ppt at the Olympic Park station, and -159.36 ppt to -25.07 ppt at the Mt. Taehwa station. This

668 is because the four following halogen reactions considered in this study contributed to better

669 $ClNO_2$ simulations: (i) $ClO + ClO \rightarrow Cl_2$; (ii) $HOBr + Cl^- \rightarrow BrCl$; (iii) different

670 parameterization of γ_{N2O5}; and (iv) $2NO_2 + Cl^- \rightarrow ClNO + NO_3^-$.

671   In addition to the evaluation of $ClNO_2$, we assessed the overall performance of the

672 implemented halogen chemistry by comparing simulated BrO and IO mixing ratios with

673 previously reported observational and modeling results. The simulated mixing ratios of BrO

674 and IO fall within the reported ranges of $0.0 - 1.3$ ppt for BrO and $0.0 - 2.5$ ppt for IO. This

675 indicates that the updated halogen processes can reasonably reproduce the regional-scale

676 behavior of bromine and iodine species.

677   Our study further emphasized the significant influences of individual halogen

678 processes on O_3 mixing ratios over South Korea. The average mixing ratios of O_3 increased by

679 ~ 0.21 ppb (0.5%) over land areas due to the impacts of chlorine and bromine processes. On

680 the contrary, the O_3 mixing ratios decreased by ~0.69 ppb (1.2%) over ocean areas due to iodine

681 processes. In addition, we quantitatively calculated the O_x budget. The net O_x production rate

682 $(P(O_x))$ increased from 3.08 to 3.33 ppb/h over the land areas and decreased from 0.21 to 0.07

683 ppb/h over the ocean areas with the simulation of the $EXP_{Cl\_Br\_I}$.

684   Finally, we further explored the impacts of full halogen processes on the atmospheric

685 composition. Compared with the CTRL simulation, the mixing ratios of HCHO and NO_x

686 increased by ~0.03 ppb (1.6%) and ~0.29 ppb (2.9%) over the land, respectively. On the other

687 hand, the mixing ratios of HO_2 and VOCs decreased by ~0.45 ppt (5.3%) and ~0.71 ppb (5.9%)

688 over the ocean areas, respectively, during the period of the KORUS-AQ campaign.

689   In conclusion, we believe that we successfully incorporated comprehensive halogen

690 processes into the CMAQ modeling system. Although our evaluation was limited to a few

691 halogen-containing species, the developed framework allowed us to explore the broader impact

692 of halogen chemistry on atmospheric composition and air quality. Despite these contributions,

693 several limitations in modeling fields remain, including (i) the spatiotemporal variability of

694 halogen emissions, (ii) incomplete or uncertain chemical mechanisms, and (iii) limited

695 observational data. In this context, further research is needed to better understand and reduce

696 these uncertainties.

697

Code and data availability

After user registration, the WRF model 3.8.1 (https://doi.org/10.5065/D6MK6B4K, WRF User Page, 2024) and CMAQ v5.2.1 (https://doi.org/10.5281/zenodo.1079909, US EPA Office of Research and Development, 2015) are available from web page. The observation data we used can be accessed at https://www-air.larc.nasa.gov/cgi-bin/ArcView/korusaq?GROUND-NIER-OLYMPIC-PARK=1 (NASA, 2019).

Author contributions

Conceptualization: KK, CHS, and KMH. Writing: KK, CHS, and KMH. Experimental design: KK, CHS, KMH, GY, and RB. Supervision: CHS. Validation: KK and CHS. Analysis: KK. Data curation: SK. All authors contributed to this paper for publication.

Competing interests

At least one of the (co-)authors is a member of the editorial board of *Atmospheric Chemistry and Physics*. The authors declare that they have no known competing financial interests or personal relationships that could have appeared to influence the work reported in this paper.

Acknowledgment

This work was supported by the National Research Foundation of Korea (NRF) grand funded by the Korea government (MSIT) (grant number: 2021R1A2C1006660).

References

Abbatt, J. and Waschewsky, G.: Heterogeneous interactions of HOBr, HNO3, O3, and NO2 with deliquescent NaCl aerosols at room temperature, J. Phys. Chem. A, 102, 3719-3725, https://doi.org/10.1021/jp980932d, 1998.

Allan, B. J., McFiggans, G., Plane, J. M., and Coe, H.: Observations of iodine monoxide in the remote marine boundary layer, J. Geophys. Res., 105, 14363-14369, https://doi.org/10.1029/1999JD901188, 2000.

Ammann, M., Cox, R. A., Crowley, J., Jenkin, M. E., Mellouki, A., Rossi, M. J., Troe, J., and Wallington, T. J.: Evaluated kinetic and photochemical data for atmospheric chemistry: Volume VI–heterogeneous reactions with liquid substrates, Atmos. Chem. Phys., 13, 8045-8228, https://doi.org/10.5194/acp-13-8045-2013, 2013.

Badia, A., Reeves, C. E., Baker, A. R., Saiz-Lopez, A., Volkamer, R., Koenig, T. K., Apel, E. C., Hornbrook, R. S., Carpenter, L. J., and Andrews, S. J.: Importance of reactive halogens in the tropical marine atmosphere: a regional modelling study using WRF-Chem, Atmos. Chem. Phys., 19, 3161-3189, https://doi.org/10.5194/acp-19-3161-2019, 2019.

Baklanov, A., Chesnokov, E., and Chichinin, A.: Rate constants for the reactions of molecular iodine with Cl, SiCl3, and SiH3 at 298 K, International Journal of Chemical Kinetics, 29, 25-33, https://doi.org/10.1002/(SICI)1097-4601(1997)29:1<25::AID-KIN4>3.0.CO;2-N, 1997.

Bedjanian, Y., Le Bras, G., and Poulet, G.: Rate constants for the reactions I+ OClO, I+ ClO, Cl+ I2, and Cl+ IO and heat of formation of IO radicals, J. Phys. Chem., 100, 15130-15136, https://doi.org/10.1021/jp960696b, 1996.

Bertram, T. and Thornton, J.: Toward a general parameterization of N2O5 reactivity on aqueous particles: the competing effects of particle liquid water, nitrate and chloride, Atmos. Chem. Phys., 9, 8351-8363, https://doi.org/10.5194/acp-9-8351-2009, 2009.

Burkholder, J., Sander, S., Abbatt, J., Barker, J., Cappa, C., Crounse, J., Dibble, T., Huie, R., Kolb, C., and Kurylo, M.: Chemical kinetics and photochemical data for use in atmospheric studies; evaluation number 19, Nasa panel for data evaluation technical report, 19-5, https://jpldataeval.jpl.nasa.gov/pdf/NASA-JPL%20Evaluation%2019-5.pdf, 2020.

Byun, D. and Schere, K. L.: Review of the governing equations, computational algorithms, and other components of the Models-3 Community Multiscale Air Quality (CMAQ) modeling system, Appl. Mech. Rev., 59, 51-77, https://doi.org/10.1115/1.2128636, 2006.

Caram, C., Szopa, S., Cozic, A., Bekki, S., Cuevas, C. A., and Saiz-Lopez, A.: Sensitivity of tropospheric ozone to halogen chemistry in the chemistry–climate model LMDZ-INCA vNMHC, Geosci. Model Dev., 16, 4041-4062, https://doi.org/10.5194/gmd-16-4041-2023, 2023.

Carter, W. P.: Development of the SAPRC-07 chemical mechanism, Atmos. Environ., 44, 5324-5335, https://doi.org/10.1016/j.atmosenv.2010.01.026, 2010.

Chang, W. L., Brown, S. S., Stutz, J., Middlebrook, A. M., Bahreini, R., Wagner, N. L., Dubé, W. P., Pollack, I. B., Ryerson, T. B., and Riemer, N.: Evaluating N2O5 heterogeneous hydrolysis parameterizations for CalNex 2010, J. Geophys. Res., 121, 5051-5070, https://doi.org/10.1002/2015JD024737, 2016.

Chen, H., Liu, P., Wang, Q., Huang, R., and Sarwar, G.: Impact and pathway of halogens on atmospheric oxidants in coastal city clusters in the Yangtze River Delta region in China, Atmospheric pollution research, 15, 101979, https://doi.org/10.1016/j.apr.2023.101979, 2024.

Chen, Q., Xia, M., Peng, X., Yu, C., Sun, P., Li, Y., Liu, Y., Xu, Z., Xu, Z., and Wu, R.: Large daytime molecular chlorine missing source at a suburban site in East China, J. Geophys. Res., 127, e2021JD035796, https://doi.org/10.1029/2021JD035796, 2022.

Clyne, M. and Cruse, H.: Atomic resonance fluorescence spectrometry for rate constants of rapid bimolecular reactions. Part 1.—Reactions O+ NO 2, Cl+ ClNO, Br+ ClNO, J. Chem. Soc. Faraday Trans., 68, 1281-1299, https://doi.org/10.1039/F29726801281, 1972.

Crawford, J. H., Ahn, J.-Y., Al-Saadi, J., Chang, L., Emmons, L. K., Kim, J., Lee, G., Park, J.-H., Park, R. J., and Woo, J. H.: The Korea–United States air quality (KORUS-AQ) field study, Elem Sci Anth, 9, 00163, https://doi.org/10.1525/elementa.2020.00163, 2021.

Deiber, G., George, C., Le Calvé, S., Schweitzer, F., and Mirabel, P.: Uptake study of ClONO 2 and BrONO 2 by Halide containing droplets, Atmos. Chem. Phys., 4, 1291-1299, https://doi.org/10.5194/acp-4-1291-2004, 2004.

Deng, S., Shi, Y., Liu, Y., Zhang, C., Wang, X., Cao, Q., Li, S., and Zhang, F.: Emission characteristics of Cd, Pb and Mn from coal combustion: Field study at coal-fired power plants in China, Fuel Processing Technology, 126, 469-475, https://doi.org/10.1016/j.fuproc.2014.06.009, 2014.

Edwards, P. M. and Young, C. J.: Primary Radical Effectiveness: Do the Different Chemical Reactivities of Hydroxyl and Chlorine Radicals Matter for Tropospheric Oxidation?, ACS ES&T Air, https://doi.org/10.1021/acsestair.3c00108, 2024.

Evans, M. J. and Jacob, D. J.: Impact of new laboratory studies of N2O5 hydrolysis on global model budgets of tropospheric nitrogen oxides, ozone, and OH, Geophys. Res. Lett., 32, https://doi.org/10.1029/2005GL022469, 2005.

Fan, S. and Li, Y.: The impacts of marine-emitted halogens on OH radicals in East Asia during summer, Atmos. Chem. Phys., 22, 7331-7351, https://doi.org/10.5194/acp-22-7331-2022, 2022.

Fernandez, R. P., Salawitch, R., Kinnison, D. E., Lamarque, J.-F., and Saiz-Lopez, A.: Bromine partitioning in the tropical tropopause layer: implications for stratospheric injection, Atmos. Chem. Phys., 14, 13391-13410, https://doi.org/10.5194/acp-14-13391-2014, 2014.

Gantt, B., Sarwar, G., Xing, J., Simon, H., Schwede, D., Hutzell, W. T., Mathur, R., and Saiz-Lopez, A.: The impact of iodide-mediated ozone deposition and halogen chemistry on surface ozone concentrations across the continental United States, Environ. Sci. Technol., 51, 1458-1466, https://doi.org/10.1021/acs.est.6b03556, 2017.

Giri, B. R., Farooq, A., Szőri, M., and Roscoe, J. M.: The kinetics of the reactions of Br atoms with the xylenes: an experimental and theoretical study, Phys. Chem. Chem. Phys., 24, 4843-4858, https://doi.org/10.1039/D1CP03740D, 2022.

Großmann, K., Frieß, U., Peters, E., Wittrock, F., Lampel, J., Yilmaz, S., Tschritter, J., Sommariva, R., Von Glasow, R., and Quack, B.: Iodine monoxide in the Western Pacific marine boundary layer, Atmos. Chem. Phys., 13, 3363-3378, https://doi.org/10.5194/acp-13-3363-2013, 2013.

Guenther, A., Jiang, X., Heald, C. L., Sakulyanontvittaya, T., Duhl, T. a., Emmons, L., and Wang, X.: The Model of Emissions of Gases and Aerosols from Nature version 2.1 (MEGAN2. 1): an extended and updated framework for modeling biogenic emissions, Geosci. Model Dev., 5, 1471-1492, https://doi.org/10.5194/gmd-5-1471-2012, 2012.

Herrmann, M., Schöne, M., Borger, C., Warnach, S., Wagner, T., Platt, U., and Gutheil, E.: Ozone depletion events in the Arctic spring of 2019: a new modeling approach to bromine emissions, Atmos. Chem. Phys., 22, 13495-13526, https://doi.org/10.5194/acp-22-13495-2022, 2022.

Huang, Y., Lu, X., Fung, J. C., Sarwar, G., Li, Z., Li, Q., Saiz-Lopez, A., and Lau, A. K.: Effect of bromine and iodine chemistry on tropospheric ozone over Asia-Pacific using the CMAQ model, Chemosphere, 262, 127595, https://doi.org/10.1016/j.chemosphere.2020.127595, 2021.

Hutzell, W., Luecken, D., Appel, K., and Carter, W.: Interpreting predictions from the SAPRC07 mechanism based on regional and continental simulations, Atmos. Environ., 46, 417-429, https://doi.org/10.1016/j.atmosenv.2011.09.030, 2012.

Iglesias-Suarez, F., Badia, A., Fernandez, R. P., Cuevas, C. A., Kinnison, D. E., Tilmes, S., Lamarque, J.-F., Long, M. C., Hossaini, R., and Saiz-Lopez, A.: Natural halogens buffer tropospheric ozone in a changing climate, Nature Climate Change, 10, 147-154, https://doi.org/10.1038/s41558-019-0675-6, 2020.

Inamdar, S., Tinel, L., Chance, R., Carpenter, L. J., Sabu, P., Chacko, R., Tripathy, S. C., Kerkar, A. U., Sinha, A. K., and Bhaskar, P. V.: Estimation of reactive inorganic iodine fluxes in the Indian and Southern Ocean marine boundary layer, Atmospheric Chemistry and Physics Discussions, 2020, 1-57, https://doi.org/10.5194/acp-20-12093-2020, 2020.

Jeong, D., Seco, R., Gu, D., Lee, Y., Nault, B. A., Knote, C. J., Mcgee, T., Sullivan, J. T., Jimenez, J. L., and Campuzano-Jost, P.: Integration of airborne and ground observations of nitryl chloride in the Seoul metropolitan area and the implications on regional oxidation capacity during KORUS-AQ 2016, Atmos. Chem. Phys., 19, 12779-12795, https://doi.org/10.5194/acp-19-12779-2019, 2019.

Jiang, J., Hao, J., Wu, Y., Streets, D. G., Duan, L., and Tian, H.: Development of mercury emission inventory from coal combustion in China, Environ. Sci., 26, 34-39, https://doi.org/10.13227/j.hjkx.2005.02.007, 2005 (in Chinese).

Jo, H.-Y., Park, J., Heo, G., Lee, H.-J., Jeon, W., Kim, J.-M., Kim, S., Kim, J.-K., Liu, Y., and Liu, P.: Interpretation of the effects of anthropogenic chlorine on nitrate formation over northeast Asia during KORUS-AQ 2016, Sci. Total Environ., 164920, https://doi.org/10.1016/j.scitotenv.2023.164920, 2023.

Keefer, R. and Andrews, L.: The interaction of bromine with benzene and certain of its derivatives, J. Am. Chem. Soc., 72, 4677-4681, https://doi.org/10.1021/ja01166a091, 1950.

Khamaganov, V. and Crowley, J.: Rate coefficients for the reactions CH3+ Br2 (224–358 K), CH3CO+ Br2 (228 and 298 K), and Cl+ Br2 (228 and 298 K), International Journal of Chemical Kinetics, 42, 575-585, https://doi.org/10.1002/kin.20505, 2010.

Kim, H., Park, R. J., Kim, S., Jeong, J. I., Jeong, D., Fu, X., and Cho, S.: Effect of nitryl chloride chemistry on air quality in South Korea during the KORUS-AQ campaign, Atmos. Environ., 312, 120045, https://doi.org/10.1016/j.atmosenv.2023.120045, 2023.

Kim, W., Moon, J.-E., Park, Y.-J., and Ishizaka, J.: Evaluation of chlorophyll retrievals from Geostationary Ocean color imager (GOCI) for the north-east Asian region, Remote Sens. Environ., 184, 482-495, https://doi.org/10.1016/j.rse.2016.07.031, 2016.

Koenig, T. K., Volkamer, R., Baidar, S., Dix, B., Wang, S., Anderson, D. C., Salawitch, R. J., Wales, P. A., Cuevas, C. A., and Fernandez, R. P.: BrO and inferred Br y profiles over the western Pacific: relevance of inorganic bromine sources and a Br y minimum in the aged tropical tropopause layer, Atmos. Chem. Phys., 17, 15245-15270, https://doi.org/10.5194/acp-17-15245-2017, 2017.

Le Breton, M., Bannan, T. J., Shallcross, D. E., Khan, M. A., Evans, M. J., Lee, J., Lidster, R., Andrews, S., Carpenter, L. J., and Schmidt, J.: Enhanced ozone loss by active inorganic bromine chemistry in the tropical troposphere, Atmos. Environ., 155, 21-28, https://doi.org/10.1016/j.atmosenv.2017.02.003, 2017.

Li, Q., Borge, R., Sarwar, G., de la Paz, D., Gantt, B., Domingo, J., Cuevas, C. A., and Saiz-Lopez, A.: Impact of halogen chemistry on summertime air quality in coastal and continental Europe: application of the CMAQ model and implications for regulation, Atmos. Chem. Phys., 19, 15321-15337, https://doi.org/10.5194/acp-19-15321-2019, 2019.

Li, Q., Zhang, L., Wang, T., Tham, Y. J., Ahmadov, R., Xue, L., Zhang, Q., and Zheng, J.: Impacts of heterogeneous uptake of dinitrogen pentoxide and chlorine activation on ozone and reactive nitrogen partitioning: improvement and application of the WRF-Chem model in southern China, Atmos. Chem. Phys., 16, 14875-14890, https://doi.org/10.5194/acp-16-14875-2016, 2016.

Li, Q., Fernandez, R. P., Hossaini, R., Iglesias-Suarez, F., Cuevas, C. A., Apel, E. C., Kinnison, D. E., Lamarque, J.-F., and Saiz-Lopez, A.: Reactive halogens increase the global methane lifetime and radiative forcing in the 21st century, Nat. Commun., 13, 2768, https://doi.org/10.1038/s41467-022-30456-8, 2022.

Li, Q., Badia, A., Wang, T., Sarwar, G., Fu, X., Zhang, L., Zhang, Q., Fung, J., Cuevas, C. A., and Wang, S.: Potential effect of halogens on atmospheric oxidation and air quality in China, J. Geophys. Res., 125, e2019JD032058, https://doi.org/10.1029/2019JD032058, 2020.

Li, Q., Fu, X., Peng, X., Wang, W., Badia, A., Fernandez, R. P., Cuevas, C. A., Mu, Y., Chen, J., and Jimenez, J. L.: Halogens enhance haze pollution in China, Environ. Sci. Technol., 55, 13625-13637, https://doi.org/10.1021/acs.est.1c01949, 2021.

Liss, P. S., Marandino, C. A., Dahl, E. E., Helmig, D., Hintsa, E. J., Hughes, C., Johnson, M. T., Moore, R. M., Plane, J. M., and Quack, B.: Short-lived trace gases in the surface ocean and the atmosphere, Ocean-atmosphere Interactions of Gases and Particles, 1-54, https://doi.org/10.1007/978-3-642-25643-1_1, 2014.

Liu, L., Bei, N., Wu, J., Liu, S., Zhou, J., Li, X., Yang, Q., Feng, T., Cao, J., and Tie, X.: Effects of stabilized Criegee intermediates (sCIs) on sulfate formation: a sensitivity analysis during summertime in Beijing–Tianjin–Hebei (BTH), China, Atmos. Chem. Phys., 19, 13341-13354, https://doi.org/10.5194/acp-19-13341-2019, 2019.

Liu, T. and Abbatt, J. P.: An experimental assessment of the importance of S (IV) oxidation by hypohalous acids in the marine atmosphere, Geophys. Res. Lett., 47, e2019GL086465, https://doi.org/10.1029/2019GL086465, 2020.

Liu, Y., Fan, Q., Chen, X., Zhao, J., Ling, Z., Hong, Y., Li, W., Chen, X., Wang, M., and Wei, X.: Modeling the impact of chlorine emissions from coal combustion and prescribed waste incineration on tropospheric ozone formation in China, Atmos. Chem. Phys., 18, 2709-2724, https://doi.org/10.5194/acp-18-2709-2018, 2018.

Mahajan, A. S., Li, Q., Inamdar, S., Ram, K., Badia, A., and Saiz-Lopez, A.: Modelling the impacts of iodine chemistry on the northern Indian Ocean marine boundary layer, Atmos. Chem. Phys., 21, 8437-8454, https://doi.org/10.5194/acp-21-8437-2021, 2021.

Mahajan, A. S., Plane, J., Oetjen, H., Mendes, L., Saunders, R., Saiz-Lopez, A., Jones, C., Carpenter, L., and McFiggans, G.: Measurement and modelling of tropospheric reactive halogen species over the tropical Atlantic Ocean, Atmos. Chem. Phys., 10, 4611-4624, https://doi.org/doi.org/10.5194/acp-10-4611-2010, 2010.

Mahajan, A. S., Gómez Martín, J. C., Hay, T. D., Royer, S. J., Yvon-Lewis, S., Liu, Y., Hu, L., Prados-Roman, C., Ordóñez, C., Plane, J. M. C., and Saiz-Lopez, A.: Latitudinal distribution of reactive iodine in the Eastern Pacific and its link to open ocean sources, Atmos. Chem. Phys., 12, 11609-11617, https://doi.org/10.5194/acp-12-11609-2012, 2012.

McDuffie, E. E., Fibiger, D. L., Dubé, W. P., Lopez-Hilfiker, F., Lee, B. H., Thornton, J. A., Shah, V., Jaeglé, L., Guo, H., and Weber, R. J.: Heterogeneous N2O5 uptake during winter: Aircraft measurements during the 2015 WINTER campaign and critical evaluation of current parameterizations, J. Geophys. Res., 123, 4345-4372, https://doi.org/10.1002/2018JD028336, 2018.

O'Reilly, J. E. and Werdell, P. J.: Chlorophyll algorithms for ocean color sensors-OC4, OC5 & OC6, Remote Sens. Environ., 229, 32-47, https://doi.org/10.1016/j.rse.2019.04.021, 2019.

Park, M.-O., Shin, W.-C., Son, Y.-B., and Noh, T.-G.: Spatial Variability of in situ and GOCI and MODIS Chlorophyll and CDOM in Summer at the East Sea, Journal of the Korean Society of Marine Environment & Safety, 21, 327-338, https://doi.org/10.7837/kosomes.2015.21.4.327, 2015.

Parrella, J., Jacob, D. J., Liang, Q., Zhang, Y., Mickley, L. J., Miller, B., Evans, M., Yang, X., Pyle, J., and Theys, N.: Tropospheric bromine chemistry: implications for present and pre-industrial ozone and mercury, Atmos. Chem. Phys., 12, 6723-6740, https://doi.org/10.5194/acp-12-6723-2012, 2012.

PENG, B.-x. and WU, D.-s.: Distribution and content of bromine in Chinese coals, Journal of Fuel Chemistry and Technology, 42, 769-773, https://doi.org/10.1016/S1872-5813(14)60034-7, 2014.

Peng, X., Wang, T., Wang, W., Ravishankara, A., George, C., Xia, M., Cai, M., Li, Q., Salvador, C. M., and Lau, C.: Photodissociation of particulate nitrate as a source of daytime tropospheric Cl2, Nat. Commun., 13, 939, https://doi.org/10.6084/m9.figshare.17099252, 2022.

Peters, C., Pechtl, S., Stutz, J., Hebestreit, K., Hönninger, G., Heumann, K., Schwarz, A., Winterlik, J., and Platt, U.: Reactive and organic halogen species in three different European coastal environments, Atmos. Chem. Phys., 5, 3357-3375, https://doi.org/10.5194/acp-5-3357-2005, 2005.

Prados-Román, C., Cuevas, C. A., Hay, T., Fernández, R. P., Mahajan, A. S., Royer, S.-J., Galí, M., Simó, R., Dachs, J., and Großmann, K.: Iodine oxide in the global marine boundary layer, Atmos. Chem. Phys., 15, 583-593, https://doi.org/10.5194/acp-15-583-2015, 2015.

Pratte, P. and Rossi, M. J.: The heterogeneous kinetics of HOBr and HOCl on acidified sea salt and model aerosol at 40–90% relative humidity and ambient temperature, Phys. Chem. Chem. Phys., 8, 3988-4001, https://doi.org/10.1039/B604321F, 2006.

Qiu, X., Ying, Q., Wang, S., Duan, L., Wang, Y., Lu, K., Wang, P., Xing, J., Zheng, M., and Zhao, M.: Significant impact of heterogeneous reactions of reactive chlorine species on summertime atmospheric ozone and free-radical formation in north China, Sci. Total Environ., 693, 133580, https://doi.org/10.1016/j.scitotenv.2019.133580, 2019a.

Qiu, X., Ying, Q., Wang, S., Duan, L., Zhao, J., Xing, J., Ding, D., Sun, Y., Liu, B., and Shi, A.: Modeling the impact of heterogeneous reactions of chlorine on summertime nitrate formation in Beijing, China, Atmos. Chem. Phys., 19, 6737-6747, https://doi.org/10.5194/acp-19-6737-2019, 2019b.

Read, K. A., Mahajan, A. S., Carpenter, L. J., Evans, M. J., Faria, B. V., Heard, D. E., Hopkins, J. R., Lee, J. D., Moller, S. J., and Lewis, A. C.: Extensive halogen-mediated ozone destruction over the tropical Atlantic Ocean, Nature, 453, 1232-1235, https://doi.org/10.1038/nature07035, 2008.

Riedel, T., Bertram, T., Ryder, O., Liu, S., Day, D., Russell, L., Gaston, C., Prather, K., and Thornton, J.: Direct N 2 O 5 reactivity measurements at a polluted coastal site, Atmos. Chem. Phys., 12, 2959-2968, https://doi.org/10.5194/acp-12-2959-2012, 2012a.

Riedel, T. P., Bertram, T. H., Crisp, T. A., Williams, E. J., Lerner, B. M., Vlasenko, A., Li, S.-M., Gilman, J., De Gouw, J., and Bon, D. M.: Nitryl chloride and molecular chlorine in the coastal marine boundary layer, Environ. Sci. Technol., 46, 10463-10470, https://doi.org/10.1021/es204632r, 2012b.

Riemer, N., Vogel, H., Vogel, B., Schell, B., Ackermann, I., Kessler, C., and Hass, H.: Impact of the heterogeneous hydrolysis of N2O5 on chemistry and nitrate aerosol formation in the lower troposphere under photosmog conditions, J. Geophys. Res. -Atmos., 108, https://doi.org/10.1029/2002JD002436, 2003.

Roberts, J. M., Osthoff, H. D., Brown, S. S., Ravishankara, A., Coffman, D., Quinn, P., and Bates, T.: Laboratory studies of products of N2O5 uptake on Cl− containing substrates, Geophys. Res. Lett., 36, https://doi.org/10.1029/2009GL040448, 2009.

Saiz-Lopez, A., Fernandez, R. P., Ordóñez, C., Kinnison, D. E., Gómez Martín, J., Lamarque, J.-F., and Tilmes, S.: Iodine chemistry in the troposphere and its effect on ozone, Atmos. Chem. Phys., 14, 13119-13143, https://doi.org/10.5194/acp-14-13119-2014, 2014.

Saiz-Lopez, A., Fernandez, R. P., Li, Q., Cuevas, C. A., Fu, X., Kinnison, D. E., Tilmes, S., Mahajan, A. S., Gómez Martín, J. C., and Iglesias-Suarez, F.: Natural short-lived halogens exert an indirect cooling effect on climate, Nature, 618, 967-973, https://doi.org/10.1038/s41586-023-06119-z, 2023.

Saiz-Lopez, A., Lamarque, J.-F., Kinnison, D. E., Tilmes, S., Ordóñez, C., Orlando, J. J., Conley, A. J., Plane, J., Mahajan, A. S., and Sousa Santos, G.: Estimating the climate significance of halogen-driven ozone loss in the tropical marine troposphere, Atmos. Chem. Phys., 12, 3939-3949, https://doi.org/10.5194/acp-12-3939-2012, 2012.

Sander, S., Friedl, R., Golden, D., Kurylo, M., Moortgat, G., Wine, P., Ravishankara, A., Kolb, C., Molina, M., and Finlyason-Pitts, B.: Chemical kinetics and photochemical data for use in atmospheric studies: Evaluation number 15, Pasadena, CA: Jet Propulsion Laboratory, California Institute of Technology2010.

Sarwar, G., Simon, H., Bhave, P., and Yarwood, G.: Examining the impact of heterogeneous nitryl chloride production on air quality across the United States, Atmos. Chem. Phys., 12, 6455-6473, https://doi.org/10.5194/acp-12-6455-2012, 2012.

Sarwar, G., Gantt, B., Schwede, D., Foley, K., Mathur, R., and Saiz-Lopez, A.: Impact of enhanced ozone deposition and halogen chemistry on tropospheric ozone over the Northern Hemisphere, Environ. Sci. Technol., 49, 9203-9211, https://doi.org/10.1021/acs.est.5b01657, 2015.

Sarwar, G., Gantt, B., Foley, K., Fahey, K., Spero, T. L., Kang, D., Mathur, R., Foroutan, H., Xing, J., and Sherwen, T.: Influence of bromine and iodine chemistry on annual, seasonal, diurnal, and background ozone: CMAQ simulations over the Northern Hemisphere, Atmos. Environ., 213, 395-404, https://doi.org/10.1016/j.atmosenv.2019.06.020, 2019.

Sherwen, T., Evans, M., Carpenter, L., Andrews, S., Lidster, R., Dix, B., Koenig, T., Sinreich, R., Ortega, I., and Volkamer, R.: Iodine's impact on tropospheric oxidants: a global model study in GEOS-Chem, Atmos. Chem. Phys., 16, 1161-1186, https://doi.org/10.5194/acp-16-1161-2016, 2016.

Simpson, W. R., Brown, S. S., Saiz-Lopez, A., Thornton, J. A., and von Glasow, R.: Tropospheric halogen chemistry: Sources, cycling, and impacts, Chem. Rev., 115, 4035-4062, https://doi.org/10.1021/cr5006638, 2015.

Skamarock, W. C., Klemp, J. B., Dudhia, J., Gill, D. O., Barker, D. M., Duda, M. G., Huang, X.-Y., Wang, W., and Powers, J. G.: A description of the advanced research WRF version 3, NCAR technical note, 475, 10.5065, https://doi.org/10.5065/D68S4MVH, 2008.

Slusher, D. L., Huey, L. G., Tanner, D. J., Flocke, F. M., and Roberts, J. M.: A thermal dissociation–chemical ionization mass spectrometry (TD-CIMS) technique for the simultaneous measurement of peroxyacyl nitrates and dinitrogen pentoxide, J. Geophys. Res., 109, https://doi.org/10.1029/2004JD004670, 2004.

Son, H.-J.: Long-term variations of phytoplankton biomass and water quality in the downstream of Nakdong River, Journal of Korean Society of Environmental Engineers, 35, 263-267, https://doi.org/10.4491/KSEE.2024.46.11.687, 2013.

Stone, D., Sherwen, T., Evans, M. J., Vaughan, S., Ingham, T., Whalley, L. K., Edwards, P. M., Read, K. A., Lee, J. D., and Moller, S. J.: Impacts of bromine and iodine chemistry on tropospheric OH and HO 2: comparing observations with box and global model perspectives, Atmos. Chem. Phys., 18, 3541-3561, https://doi.org/10.5194/acp-18-3541-2018, 2018.

Takashima, H., Kanaya, Y., Kato, S., Friedrich, M. M., Van Roozendael, M., Taketani, F., Miyakawa, T., Komazaki, Y., Cuevas, C. A., and Saiz-Lopez, A.: Full latitudinal marine atmospheric measurements of iodine monoxide, Atmospheric Chemistry and Physics Discussions, 2021, 1-24, https://doi.org/10.5194/acp-22-4005-2022, 2021.

von Glasow, R. and Crutzen, P. J.: Tropospheric halogen chemistry, Treatise on Geochemistry, 4, 347, 2003.

Wang, X., Jacob, D. J., Downs, W., Zhai, S., Zhu, L., Shah, V., Holmes, C. D., Sherwen, T., Alexander, B., and Evans, M. J.: Global tropospheric halogen (Cl, Br, I) chemistry and its impact on oxidants, Atmos. Chem. Phys., 21, 13973-13996, https://doi.org/10.5194/acp-21-13973-2021, 2021.

Wang, X., Wang, H., Xue, L., Wang, T., Wang, L., Gu, R., Wang, W., Tham, Y. J., Wang, Z., and Yang, L.: Observations of N2O5 and ClNO2 at a polluted urban surface site in North China: High N2O5 uptake coefficients and low ClNO2 product yields, Atmos. Environ., 156, 125-134, https://doi.org/10.1016/j.atmosenv.2017.02.035, 2017.

Wiedinmyer, C., Akagi, S., Yokelson, R. J., Emmons, L., Al-Saadi, J., Orlando, J., and Soja, A.: The Fire INventory from NCAR (FINN): A high resolution global model to estimate the emissions from open burning, Geosci. Model Dev., 4, 625-641, https://doi.org/10.5194/gmd-4-625-2011, 2011.

Woo, J.-H., Kim, Y., Kim, H.-K., Choi, K.-C., Eum, J.-H., Lee, J.-B., Lim, J.-H., Kim, J., and Seong, M.: Development of the CREATE inventory in support of integrated climate and air quality modeling for Asia, Sustainability, 12, 7930, https://doi.org/10.3390/su12197930, 2020.

Yang, X., Cox, R. A., Warwick, N. J., Pyle, J. A., Carver, G. D., O'Connor, F. M., and Savage, N. H.: Tropospheric bromine chemistry and its impacts on ozone: A model study, J. Geophys. Res., 110, https://doi.org/10.1029/2005JD006244, 2005.

Yi, X., Yin, S., Huang, L., Li, H., Wang, Y., Wang, Q., Chan, A., Traoré, D., Ooi, M. C. G., and Chen, Y.: Anthropogenic emissions of atomic chlorine precursors in the Yangtze River Delta region, China, Sci. Total Environ., 771, 144644, https://doi.org/10.1016/j.scitotenv.2020.144644, 2021.

Yu, C., Wang, Z., Xia, M., Fu, X., Wang, W., Tham, Y. J., Chen, T., Zheng, P., Li, H., and Shan, Y.: Heterogeneous N2O5 reactions on atmospheric aerosols at four Chinese sites: improving model representation of uptake parameters, Atmos. Chem. Phys., 20, 4367-4378, https://doi.org/10.5194/acp-20-4367-2020, 2020.

Zhu, L., Jacob, D. J., Eastham, S. D., Sulprizio, M. P., Wang, X., Sherwen, T., Evans, M. J., Chen, Q., Alexander, B., and Koenig, T. K.: Effect of sea salt aerosol on tropospheric bromine chemistry, Atmos. Chem. Phys., 19, 6497-6507, https://doi.org/10.5194/acp-19-6497-2019, 2019.